# Evidence for fire in the Pliocene Arctic in response to amplified temperature

Tamara Fletcher[1*], Lisa Warden[2*], Jaap S. Sinninghe Damsté[2,3], Kendrick J. Brown[4,5], Natalia Rybczynski[6,7], John Gosse[8], and Ashley P Ballantyne[1]

[1] College of Forestry and Conservation, University of Montana, Missoula, 59812, USA
[2] Department of Marine Microbiology and Biogeochemistry, NIOZ Royal Netherlands Institute for Sea Research, Den Berg, 1790, Netherlands
[3] Department of Earth Sciences, University of Utrecht, Utrecht, 3508, Netherlands
[4] Natural Resources Canada, Canadian Forest Service, Victoria, V8Z 1M5, Canada
[5] Department of Earth, Environmental and Geographic Science, University of British Columbia Okanagan, Kelowna, V1V 1V7, Canada
[6] Department of Palaeobiology, Canadian Museum of Nature, Ottawa, K1P 6P4, Canada
[7] Department of Biology & Department of Earth Sciences, Carleton University, Ottawa, K1S 5B6, Canada
[8] Department of Earth Sciences, Dalhousie University, Halifax, B3H 4R2, Canada
*Authors contributed equally to this work

*Correspondence to*: Tamara Fletcher (tamara.fletcher@umontana.edu)

**Abstract.** The mid-Pliocene is a valuable time interval for investigating equilibrium climate at current atmospheric $CO_2$ concentrations, because atmospheric $CO_2$ concentrations are thought to have been comparable to current day and yet the climate and distribution of ecosystems were quite different. One intriguing, but not fully understood, feature of the early to mid-Pliocene climate is the amplified arctic temperature response and its impact on arctic ecosystems. Only the most recent models appear to correctly estimate the degree of warming in the Pliocene Arctic and validation of the currently proposed feedbacks is limited by scarce terrestrial records of climate and environment. Here we reconstruct the summer temperature and fire regime from a sub-fossil fen-peat deposit on west-central Ellesmere Island, Canada, that has been chronologically constrained using cosmogenic nuclide burial dating to 3.9 +1.5/-0.5 Ma.

The estimate for average mean summer temperature is 15.4±0.8°C using specific bacterial membrane lipids, i.e. branched glycerol dialkyl glycerol tetraethers. This is above the proposed threshold that predicts a substantial increase in wildfire in the modern high-latitudes. Macro-charcoal was present in all samples from this Pliocene section with notably higher charcoal concentration in the upper part of the sequence. This change in charcoal was synchronous with a change in vegetation that included an increase in abundance of fire-promoting *Pinus* and *Picea*. Paleovegetation reconstructions are consistent with warm summer temperatures, relatively low summer precipitation and an incidence of fire comparable to fire adapted boreal forests of North America, and central Siberia.

To our knowledge, this site provides the northern-most evidence of fire during the Pliocene. It suggests that ecosystem productivity was greater than present-day, providing fuel for wildfires, and that the climate was conducive to the ignition of fire during this period. The results reveal interactions between paleovegetation and paleoclimate were mediated by fire in the High Arctic during the Pliocene, even though $CO_2$ concentrations were similar to modern.

## 1 Introduction

Current rates of warming in the Canadian Arctic are now roughly triple the rate of global warming (Bush and Lemmen, 2019). Since 1850, global land surface temperatures have increased by approximately 1.0°C, whereas circum-arctic land surface temperatures have increased by >2.0°C (Jones and Moberg, 2003; Francis and Skific, 2015). Such arctic amplification of temperatures has also occurred during other warm climate anomalies in Earth's past. Paleoclimate records from the Arctic indicate that the change in arctic summer temperatures during past global warm periods was 3–4 times larger than global temperature change (Miller et al., 2010). While earth system models (ESMs) have been able to provide fairly accurate predictions of the modern amplification of arctic temperatures hitherto observed for some time (Marshall et al., 2014), they have only recently implemented mechanisms that simulate Arctic amplification of temperature for past warm periods such as the Pliocene (2.6–5.3) with a convincing pattern of seasonality (Zheng et al. 2019). The success of earlier models at capturing modern warming, contrasted with the additions needed to simulate the Pliocene Arctic temperatures, suggest that the array of fast and slow feedback mechanisms have not fully manifested for the modern Arctic, and perhaps there are still further feedback mechanisms we are yet to understand and implement in climate models.

The Pliocene is an intriguing climatic interval that offers important insights into climate feedbacks. Atmospheric $CO_2$ concentrations were, at times, as high as modern (Fig. 1), but generally show a decreasing trend throughout the Pliocene (Haywood et al., 2016; Pagani et al., 2010; Royer et al., 2007; Stap et al., 2016), Although $CO_2$ estimates from different methods do not converge, the modelled direct effects of these $CO_2$ discrepancies appear to be small (Feng et al., 2017). Of additional importance for comparability to the modern climate system, continental configurations were similar to present (Dowsett et al., 2016). While global mean annual temperatures (MATs) during the Pliocene were only ~ 3°C warmer than present day, arctic land surface MATs may have been as much as 15 to 22°C warmer (Ballantyne et al., 2010; Csank et al., 2011a; Csank et al., 2011b; Fletcher et al., 2017). Further, arctic sea surface temperatures may have been as much as 10 to 15°C warmer than modern (Robinson, 2009), and sea-levels were approximately 25m higher than present (Dowsett et al., 2016). As a result, the Arctic terrestrial environment was significantly different from today, with boreal ecosystems at much higher latitudes (Salzmann et al., 2008). These changes in vegetation due to climate, may have also provided further important feedbacks to arctic temperatures (e.g. Otto-Bliesner and Upchurch Jr, 1997).

To advance our understanding of arctic ecosystem response and feedback to temperature amplification during past warm intervals in Earth's history this investigation targets an exceptionally well-preserved arctic sedimentary sequence to simultaneously reconstruct summer temperature, vegetation and fire from a single site.

## 2 Methods

### 2.1 Site description

To investigate the environment and climate of the Pliocene Arctic we focused on the Beaver Pond (BP) fossil site, located at 78° 33′ N (Fig. 2) on Ellesmere Island. The stratigraphic section located at ~380 meters above sea level (MASL) today includes unconsolidated bedded sands and gravels, and rich organic layers including a fossil rich peat

layer, up to 2.4 m thick, with sticks gnawed by an extinct beaver (*Dipoides spp.*). The assemblage of fossil plants and animals at BP has been studied extensively to gain insight into the past climate and ecology of the Canadian High Arctic (Ballantyne et al., 2006; Csank et al., 2011a; Csank et al., 2011b; Fletcher et al., 2017; Mitchell et al., 2016; Rybczynski et al., 2013; Tedford and Harington, 2003; Wang et al., 2017). Previous paleoenvironmental evidence suggests the main peat unit is a rich fen deposit with a neutral to alkaline pH, associated with open water (Mitchell et al., 2016), likely a lake edge fen or shallow lake fen, within a larch-dominated forest-tundra environment (Matthews and Fyles, 2000), not a low pH peat-bog. While the larch species identified at the site, *Larix groenlandia*, is extinct (Matthews and Fyles, 2000), many other plant remains are Pliocene examples of taxa that are extant (Fletcher et al., 2017).

The fen-peat unit examined in this study was sampled in 2006 and 2010. The main sequence examined across the methods used in this study includes material from Unit II, the entire span of Unit III, and material from Unit IV sampled from Section A as per Mitchell et al. (2016; Fig. S1; see Mitchell et al. 2016 Fig 5), with a total sampled profile of 1.65 m. Unit III has been estimated to represent ~20 000 years of deposition based on modern northern fen accumulation rates (Mitchell et al., 2016). The charcoal counts and measurements from this locality were based on 31 sample layers from the 2006 field campaign, while the temperature estimates from specific bacterial membrane lipids were taken from 22 of the sample layers collected in 2006 and an additional 12 samples collected in 2010. The same samples from the 2006 season were analyzed for mean summer temperature and char count where contents of the sample allowed. Pollen was tabulated from 10 samples from the 2006 sequence, located at different stratigraphic depths.

### 2.2 Geochronology

While direct dating of the peat was not possible, we were able to establish a burial age for fluvial sediments deposited approximately 4–5 m above and 30 m to the southwest of the peat. We used a method based on the ratio of isotopes produced in quartz by secondary cosmic rays. The cosmogenic nuclide burial dating approach measures the ratio of cosmogenic $^{26}$Al ($t_{½}$ = 0.71 Ma) and $^{10}$Be ($t_{½}$ = 1.38 Ma) in quartz sand grains that were exposed on hillslopes and alluvium prior to final deposition at BP. Once the quartz grains are completely shielded from cosmic rays, the ratio of the pair will predictably decrease because $^{26}$Al has double the radiodecay rate of $^{10}$Be. In 2008, four of the medium to coarse grained quartz samples were collected from a vertical profile of planar crossbedded fluvial sands between 8.7 and 10.4 m below the overlying till surface. The samples were 5 cm thick, separated by an average of 62 cm, and should closely date the peat (the sandy braided stream beds represent on the order of ~$10^4$ years from the top of the peat to the highest sample). Quartz concentrates were extracted from the arkosic sediment using Frantz magnetic separation, heavy liquids, and differential leaching with HF in ultrasonic baths. When sample aliquots reached aluminum concentrations <100 ppm (ICP-OES) as a proxy of feldspar abundance, the quartz concentrate was subjected to a series of HF digestion and rinsing steps to ensure that more than 30% of the quartz had been dissolved to remove meteoric $^{10}$Be. Approximately 200 mg of Be extracted from a Homestake Gold Mine beryl-based carrier was added to 150 g of each quartz concentrate (no Al carrier was needed for these samples). Such large quartz masses were digested because of the uncertainty in the abundance of the faster decaying isotope. Following repeated

perchloric-acid dry-downs to remove unreacted HF, pH-controlled precipitation, column chemistry ion chromatography to extract the Be and Al ions, precipitation in ultrapure ammonia gas, and calcination at temperatures above 1000°C in a Bunsen flame for three minutes, oxides were mixed with equal amounts of niobium and silver by volume. These were packed into stainless steel targets for measurement at Lawrence Livermore National Laboratory's accelerator mass spectrometer (AMS). Uncertainty estimates for $^{26}Al/^{10}Be$ were calculated as 1σ by combining AMS precision with geochemistry errors in quadrature. For a complete detailed description of TCN methods see Rybczynski et al. (2013). The ages provided here are updated from Rybczynski et al. (2013) by using more recent production rate information and considering the potential for increasing exposure to deeply penetrating muons during the natural post-burial exhumation at BP.

### 2.3 Paleotemperature Reconstruction

Paleotemperature estimates were determined based on the distribution of fossilized, sedimentary membrane lipids known as branched glycerol dialkyl glycerol tetraethers (brGDGTs) that are well preserved in peat bogs, soils, and lakes (Powers et al., 2004; Weijers et al., 2007c). These unique lipids are thought to be synthesized by a wide array of Acidobacteria within the soil (Sinninghe Damsté et al., 2011; Sinninghe Damsté et al., 2014) and presumably other bacteria (Sinninghe Damsté et al., 2018) in soils and peat bogs but also in aquatic systems. Previously, it has been established that the degree of methyl branching (expressed in the methylation index of branched tetraethers; MBT) is correlated with mean annual air temperature (MAAT), and the relative amount of cyclopentane moieties (expressed in the cyclization index of branched tetraethers; CBT) has been shown to correlate with both soil pH and MAAT (Weijers et al., 2007b). Because of the relationship of the distribution of these fossilized membrane lipids with these environmental parameters, the distribution of these membrane lipids has been used for paleoclimate applications in different environments including coastal marine sediments (Bendle et al., 2010; Weijers et al., 2007a), peats (Ballantyne et al., 2010; Naafs et al., 2017), paleosols (Peterse et al., 2011; Zech et al., 2012), and lacustrine sediments (Loomis et al., 2012; Niemann et al., 2012; Pearson et al., 2011; Zink et al., 2010). In this study we reconstruct mean summer air temperature (MST), using a modified version of a calibration that was developed by Pearson et al. (2011) and is based on 90 core top lacustrine sediment samples from diverse climates and geographical areas.

Improved separation methods (Hopmans et al., 2016) have recently led to the separation and quantification of the 5- and 6-methyl brGDGT isomers that used to be treated as one since the 6-methyl isomers were co-eluting with the 5-methyl isomers (De Jonge et al., 2013). This has led to the definition of new indices and improved MAAT calibrations based on the global soil (De Jonge et al., 2014), peat (Naafs et al., 2017), and African lake (Russell et al., 2018) datasets.

Sediment samples were freeze-dried and then ground and homogenized with a mortar and pestle. Next, using the Dionex™ accelerated solvent extractor (ASE), 0.5–1.0 g of sediment was extracted with the solvent mixture of dichloromethane (DCM):methanol (9:1, v/v) at a temperature of 100°C and a pressure of 1500 psi (5 min each) with 60% flush and purge 60 s. The Caliper Turbovap®LV was utilized to concentrate the collected extract, which was then transferred using DCM and dried over anhydrous $Na_2SO_4$ before being concentrated again under a gentle stream of $N_2$ gas. To quantify the amount of GDGTs, 1 µg of an internal standard (C46 GDGT; Huguet et al., 2006) was

added to the total lipid extract. Then, the total lipid extract was separated into three fractions using hexane:DCM (9:1, v:v) for the apolar fraction, hexane:DCM (1:1, v:v) for the ketone fraction and DCM:MeOH (1:1, v:v) for the polar fraction, using a column composed of $Al_2O_3$, which was activated for 2 h at 150°C. The polar fraction, which contained the GDGTs, was dried under a steady stream of $N_2$ gas and weighed before being re-dissolved in hexane:isopropoanol (99:1, v:v) at a concentration of 10 mg $ml^{-1}$ and subsequently passed through a 0.45 µm PTFE filter. Finally, the polar fractions were analyzed for GDGTs by ultra-high performance liquid chromatography – atmospheric pressure positive ion chemical ionization – mass spectrometry (UHPLC-APCI-MS) using the method described by Hopmans et al., (2016). The polar fractions of some samples were re-run on the UHPLC-APCI-MS multiple times and the average fractional abundances of the brGDGTs was determined.

For the calculation of brGDGT-based proxies, the brGDGTs are specified by the Roman numerals as indicated in Fig. S2. The 6-methyl brGDGTs are distinguished from the 5-methyl brGDGTs by a prime. The novel indices, including $MBT'_{5Me}$ based on just the 5-methyl brGDGTs and the CBT′ that was used to calculate the pH (De Jonge et al., 2014):

$$MBT'_{5Me} = ([Ia] + [Ib] + [Ic]) / ([Ia] + [Ib] + [Ic] + [IIa] + [IIb] + [IIc] + [IIIa] + [IIIb] + [IIIc]) \quad (1)$$

$$CBT' = {}^{-10}\log[([Ic] + [IIa'] + [IIb'] + [IIc'] + [IIIa'] + [IIIb'] + [IIIc'])/([Ia] + [IIa] + [IIIa])] \quad (2)$$

The square brackets denote the fractional abundance of the brGDGT within the bracket relative to the total brGDGTs. The distributions of aquatically produced brGDGTs in the lake calibration developed by Pearson et al. (2011) were used to determine MST. When this calibration is used the fractional abundances of IIa and IIa′ must be summed because these two isomers co-eluted under the chromatographic conditions used by Pearson et al. (2011):

$$MST\ (°C) = 20.9 + 98.1 \times [Ib] - 12 \times ([IIa] + [IIa']) - 20.5 \times [IIIa] \quad RMSE = 2.0°C \quad (3)$$

MAAT and surface water pH were also calculated using a novel calibration created using sediments from East African lakes analysed with the novel chromatography method and based upon $MBT'_{5Me}$ (Russell et al., 2018).

$$MAAT = -1.2141 + 32.4223 * MBT'_{5Me} \quad RMSE\ of\ 2.44\ °C \quad (4)$$

$$Surface\ water\ pH = 8.95 + 2.65 * CBT' \quad RMSE\ of\ 0.80 \quad (5)$$

Analytical error (±0.38ºC) was estimated as the average standard deviation of the duplicates run on 18 of the samples from throughout the section.

### 2.4 Vegetation and Fire Reconstruction

For charcoal, a total of thirty 2 $cm^3$ samples were taken at 5 cm intervals from depths from 380 and 381.45 MASL at the BP site, with an additional 2$cm^{-3}$ sample collected at 381.65 MASL. All samples were deflocculated using sodium hexametaphosphate and passed through 500, 250 and 125 µm nested mesh sieves. The residual sample caught on each

sieve was then collected in a gridded petri dish and examined using a stereomicroscope at 20-40X magnification to obtain charcoal concentration (fragments $cm^{-3}$). Charcoal area ($mm^2$ $cm^{-3}$) was measured for each sample using specialized imaging software from Scion Corporation. For a detailed description of methods see Brown and Power (2013).

Vegetation was reconstructed using pollen and spores (herein pollen) at selected elevations chosen to capture upper and lower sections of the elevation profile, and that corresponded with changes in charcoal. The sample depths selected for pollen analyses were 380.3–380.4 MASL, 381.10–381.25 MASL, and 381.35–381.45 MASL. Samples were processed using standard approaches (Moore et al., 1991), whereby 1cm3 sediment subsamples were treated with 5% KOH to remove humic acids and break up the samples. Carbonates were dissolved using 10% HCl, whereas silicates and organics were removed by HF and acetolysis treatment, respectively. Pollen slides were made by homogenizing 35 µl of residue, measured using a single-channel pipette, with 15 µl of melted glycerin jelly. Slides were counted using a Leica DM4000 B LED compound microscope at 400–630x magnification. A reference collection and published keys (McAndrews et al., 1973; Moore et al., 1991) aided identification.

In addition to tabulating pollen and charcoal, a list of plant taxa derived from Beaver Pond was previously compiled in Fletcher et al. (2017). Extant species from this list were selected and their modern occurrences extracted from the Global Biodiversity Information Facility (GBIF.org, 2017). Observation data was grouped by 5° latitude 5° longitude grids cells, and the shared species count calculated using R (R Core Team, 2016). Modern fire frequency was mapped using the MODIS 6 Active Fire Product. The fire pixel detection count per day, within the same 5° latitude 5° longitude grids cells was tabulated over the ten years 2006–2015, and standardized by area of the cell. The modern climate maps were generated using data from WorldClim 1.4 (Hijmans et al., 2005). The values for the bioclimatic variables mean temperature of the warmest quarter (equivalent to MST) and precipitation of the warmest quarter (summer precipitation) were also averaged by grid cell. The shared species count, climate values, and fire day detections were mapped to the northern polar stereographic projection in ArcMap 10.1.

## 3 Results

### 3.1 Geochronology

The burial dating results with $^{26}Al/^{10}Be$ in quartz sand at 10 m below modern depth provides four individual ages. From shallowest to deepest, the burial ages are 3.6 +1.5/-0.5 Ma, 3.9 +3.7/-0.5 Ma, 4.1 +5.8/-0.4 Ma, and 4.0 +1.5/-0.4 Ma (Table S2), with an unweighted mean age of 3.9 Ma. The convoluted probability distribution function yields a maximum probability age of 4.5 Ma. Unfortunately, the positive tails of the probability distribution functions of two of the samples exceeds the radiodecay saturation limit of the burial age. Therefore, their probability distributions do not reflect the actual age probabilities and uncertainty. Given the positive tail in the probability distribution functions, and the inability to convolve all samples, we recommend using the unweighted mean age, 3.9 Ma, with an uncertainty of +1.5/-0.5 Ma as indicated by the two samples with unsaturated limits. Despite the apparent upward younging of the individual burial ages, the 1σ-uncertainties overlap rendering the samples indistinguishable.

### 3.2 Paleotemperature Estimates

#### 3.2.1 Provenance of branched GDGTs

Previously, brGDGT derived MAAT estimates (-0.6 ± 5.0 °C) from BP sediments were developed using the older chromatography methods that did not separate the 5- and 6- methyl brGDGTs, and a soil calibration (Ballantyne et al., 2010). In marine and lacustrine sediments, bacterial brGDGTs were thought to originate predominantly from continental soil erosion arriving in the sediments through terrestrial runoff. More recent studies, however, have indicated aquatically produced brGDGTs could be affecting the distribution of the sedimentary brGDGTs and thus the temperature estimates based upon them (Warden et al., 2016; Zell et al., 2013; Zhu et al., 2011). Since the discovery that sedimentary brGDGTs can have varying sources, different calibrations have been developed depending on the origin of the brGDGTs, i.e. soil calibration (De Jonge et al., 2014), peat calibration (Naafs et al., 2017) and aquatic calibrations (i.e. Foster et al., 2016; Pearson et al., 2011; Russell et al., 2018). Therefore, several studies have recommended that the potential sources of the sedimentary brGDGTs should be investigated before attempting to use brGDGTs for paleoclimate applications (De Jonge et al., 2015; Warden et al., 2016; Yang et al., 2013; Zell et al., 2013). In this study, we examine the distribution of brGDGTs in an attempt to determine their origin and consequently the most appropriate calibration to utilize in order to reconstruct temperatures from the BP sediments.

Branched GDGTs IIIa and IIIa′ on average had the highest fractional abundance of the brGDGTs detected in the BP sediments (see Fig. S2 for structures; Table S4). A previous study established that when plotted in a ternary diagram the fractional abundances of the tetra-, penta- and hexamethylated brGDGTs, soils lie within a distinct area (Sinninghe Damsté, 2016). To assess whether the brGDGTs in the BP deposit were predominantly derived from soils, we compared the fractional abundances of the tetra-, penta- and hexamethylated brGDGTs in the BP sediments to those from modern datasets in a ternary diagram (Fig. 3). Since the contribution of brGDGTs from either peat or aquatic production could affect the use of brGDGTs for paleoclimate application, in addition to comparing the samples to the global soil dataset (De Jonge et al., 2014), peat and lacustrine sediment samples were added into the ternary plot to help elucidate the provenance of brGDGTs in the BP sediments. According to Sinninghe Damsté (2016), it is imperative to only compare samples in a ternary diagram like this where all of the datasets were analyzed with the novel methods that separate the 5- and 6-methyl brGDGTs since the improved separation can result in an increased quantification of hexamethylated brGDGTs. Recently, samples from East African lake sediments were analyzed using these new methods (Russell et al., 2018) and so these samples were included in the ternary plot for comparison (Fig. 3). Although the lakes from the East African dataset are all from a tropical area, they vary widely in altitude and, thus, in MAAT. We separated them into three categories by MAAT (lakes >20°C, lakes between 10-20°C and lakes<10°C). By comparing all the samples in the ternary plot, it was evident that the BP samples plotted closest to the lacustrine sediment samples from regions in East Africa with a MAAT <10°C, suggesting that the provenance of the majority of the brGDGTs from the BP sediments was not soil or peat but lacustrine aquatic production.

The average estimated surface water pH for the BP sediments (8.6±0.2) calculated using eq. (5), is within the 6 –9 range typical of lakes and rivers (Mattson, 1999). This value is near the upper limit of rich fens characterized by the presence of *S. scorpioides* (Kooijman and Westhoff, 1995; Kooijman and Paulissen, 2006) and is higher than what would be expected for peat-bog sediments that are acidic (pH 3–6; Clymo, 1964) and which constitute most of the

peats studied by Naafs et al. (2017). A predominant origin from lake aquatic production is in keeping with previous interpretation of the paleoenvironment of the BP site, which was at least at times covered by water as evidenced by fresh water diatoms, fish remains and gnawed beaver sticks in the sediment (Mitchell et al., 2016).

### 3.2.2 Aquatic Temperature Transfer Function

Since there is evidence that the majority of the brGDGTs in the BP sediments are aquatically produced, an aquatic transfer function was used for reconstructing temperature. When we apply the African lake calibration (Eq. 4), the resulting estimated MAAT for BP is 7.1 ± 1.0 °C (mean ± standard deviation). This value is high compared to other previously published estimates from varying proxies, which have estimated MAAT in this region to be in the range of -5.5 to 0.8°C, (Ballantyne et al., 2010; Ballantyne et al., 2006; Csank et al., 2011a; Csank et al., 2011b; Fletcher et al., 2017). A concern when applying this calibration is that it is based on lakes from an equatorial region that does not experience substantial seasonality, whereas, the Pliocene Arctic BP site did experience substantial seasonality (Fletcher et al., 2017). Biological production (including brGDGT production) in BP was likely skewed towards summer and, therefore, summer temperature has a larger influence on the reconstructed MAAT. Unfortunately, no global lake calibration set using individually quantified 5- and 6-methyl brGDGTs is yet available. Therefore, to calculate MST (Eq. 3) we applied the aquatic transfer function developed by Pearson et al. (2011) by combining the individual fractional abundances of the 5- and 6-methyl brGDGTs. The Pearson et al. (2011) calibration was based on a global suite of lake sediments including samples from the Arctic, thus covering a greater range of seasonal variability. The resulting average estimated MST was 15.4 ± 0.8 °C (mean ± 1 standard deviation, n = 34 samples), with temperatures ranging between 14.1 and 17.4 °C (Fig. 4). This is in good agreement with recent estimates based on Climate Reconstruction Analysis using Coexistence Likelihood Estimation (CRACLE; Fletcher et al., 2017) that concluded that MSTs at BP during the Pliocene were approximately 13 to 15°C.

## 3.3 Vegetation and Fire Reconstruction

All sediment samples from BP contained charcoal (Fig. 4), indicating the consistent prevalence of biomass burning in the High Arctic during this time period. However, counts were variable throughout the section, with the middle and lower sections (mean 34 fragments $cm^{-3}$) containing less charcoal compared to the upper section upper section (mean 444 fragments $cm^{-3}$). Overall, samples from BP contained on average 100.0 ± 165 fragments $cm^{-3}$ (mean ± 1 σ), with charcoal area averaging 12.3 ± 20.2 $mm^2$ $cm^{-3}$. The variability of charcoal within any given sample was relatively low with a 1 σ among charcoal area of approximately 2 $mm^2$ $cm^{-3}$.

The three parts of the section analysed for pollen (380.3–380.4 MASL, 381.15–381.25 MASL, and 381.35–381.45 MASL) reveal variations in vegetation (Figs. 4 and 5). Near the bottom of the section (380.3-380.4 MASL), *Larix* (26%) and *Betula* (17%) were the dominant trees. *Alnus* (6%) and *Salix* (6%) together with ericaceous pollen (4%) were relatively high. In contrast, low numbers of *Picea* (3%), *Pinus* (3%) and fern spores were recorded. Additional wetland taxa like *Myrica* (5%) and Cyperaceae (6%) were also noted. Overall, the non-arboreal (23%) signal was well developed. Crumpled and/or ruptured inaperturate grains with surface sculpturing that varied from scabrate to verricate were noted in the assemblage (12%), but could not be definitively identified. It is possible that these grains

represent *Populus*, Cupressaceae or additional Cyperaceae pollen. Between 381.10-381.25 MASL, *Larix* (38%) and *Betula* (21%) increased in abundance, followed by ferns (7%). Cyperaceae remained at similar levels (6%) whereas *Picea* and *Pinus* decreased to 2% and 1%, respectively. Unidentified inaperturate types collectively averaged 14%. *Larix* pollen (23%) remained abundant near the top of the section (381.35-381.45 MASL), whereas *Betula* (2%) decreased. *Picea* (16%) *Pinus* (6%) and ferns (23%) increased in abundance. Of the ferns, trilete spores and cf. *Botrychium* were most abundant, followed by cf. *Dryopteris*. Inaperturate unknowns (10%) were also observed. Other notables included Ericaceae (2%) and Cyperaceae (2%). While rare, Onagraceae grains were also observed (Fig. 5).

According to the GBIF-based mapping exercise, the paleofloral assemblage at BP most closely resembles modern vegetation found in northern North America, particularly on the eastern margin (e.g. New Hampshire, New Brunswick and Nova Scotia) and the western margin (Alaska, Washington, British Columbia, and Alberta; Fig. 7a), and central Fennoscandia. Of these areas, the western coast of northern North America and eastern coast of southern Sweden have the most similarity to the reconstructed BP climate in terms of MST (Fig. 7b) and summer precipitation (Fig. 7c).

While high counts of active fire days are common in the western part of the North American boreal forest, it is not as common in the eastern part of the North American boreal forest (Fig. 7d), likely due to the differences in the precipitation regime. Low fire counts also typified Fennoscandia, likely due to historical severe fire suppression (Brown and Giesecke, 2014; Niklasson and Granström, 2004). Therefore, based on our reconstruction of the climate and ecology of the BP site, our results suggest that BP most closely resembled a boreal-type forest ecosystem shaped by fire, similar to those of Washington, British Columbia, Northwest Territories, Yukon and Alaska (Figure 3; but see Sect. 4.3).

## 4 DISCUSSION

### 4.1 Geochronology

The plant and animal fossil assemblages observed at BP suggest a depositional age between 3 and 5 Ma (Matthews Jr and Ovenden, 1990; Tedford and Harington, 2003). This biostratigraphic age was corroborated with an amino-acid racemization age (>2.4 ± 0.5 Ma) and Sr-correlation age (2.8–5.1 Ma) on shells (Brigham-Grette and Carter, 1992) in biostratigraphically correlated sediments on Meighen Island, situated 375 km to the west-north-west. The previously calculated burial age of 3.4 Ma for the BP site is a minimum age because no post-depositional production of $^{26}$Al or $^{10}$Be by muons was assumed. If the samples are considered to have been buried at only the current depth (ca. 10 m, see supplemental data) then the ages plot to the left and outside of the burial field, indicating that the burial depth was significantly deeper for most of the post-depositional history. The revised cosmogenic nuclide burial age is 3.9 +1.5/-0.5 Ma. It is the best interpretation of burial age data based on improved production rate systematics (e.g. Lifton et al., 2014), and more reasonable estimates of erosion rate and ice cover since the mid-Pliocene (see Fig. S3; Table S5). As the stratigraphic position of the cosmogenic samples is very close to the BP peat layers, we interpret the age to represent the approximate time that the peat was deposited.

### 4.2 Fire, vegetation, temperature: a feedback triangle

Wildfire is a key driver of ecological processes in modern boreal forests (Flannigan et al., 2009; Ryan, 2002), and although historically rare, is becoming more frequent in the tundra in recent years (Mack et al., 2011). The modern increase in fire frequency is likely as a consequence of atmospheric $CO_2$ driven climate warming and feedbacks such as reduced sea ice extent (Hu et al., 2010), because the probability of fire is highest where temperature and moisture are conducive to growth and drying of fuels followed by conditions that favor ignition (Whitman et al., 2015). Young et al. (2017) confirmed the importance of summer warmth and moisture availability patterns in predicting fire across Alaska, highlighting a July temperature of ~13.5 °C as a key threshold for fire across Alaska.

The abundance of charcoal at BP demonstrates that climatic conditions were conducive to ignition and that sufficient biomass available for combustion existed across the landscape. brGDGTs-derived temperature estimates suggest mean summer temperatures at BP exceeded the ~13.5 °C threshold (Young et al., 2017) that drastically increases the chance of wildfire. Indeed, the estimate of ~15.4°C suggests mean reconstructed summer temperatures were ~11°C higher than modern day Eureka, Canada (~4.1°C; Fig. 2) representing substantial additional amplification compared to the global average. Without the increased arctic amplification of temperature that accompanies climate equilibrium with high $CO_2$, mean summer temperatures would be lower than the July temperature threshold that predicts increased wildfire. This is evidence that Pliocene arctic amplification of temperatures was a direct feedback to increased wildfire activity. The increased extent of boreal forest into the Arctic was also possible due to arctic amplification of temperatures. This biomass provided the fuel for combustion and thus Pliocene arctic amplification of temperatures is also an indirect feedback to wildfire (Fig. 6).

Conversely, the charcoal record at BP suggests substantial biomass burning that could have acted as a feedback mechanism amplifying or dampening warming seasonally, during the mid-Pliocene (Fig. 6). Studies of the impact of wildfire on surface energy balance in present-day northern ecosystems have revealed the complexity of predicting wildfire's impact on climate. Ecosystems exhibit changing responses through time from the scale of years post-burning (Randerson et al. 2006; Bonan, 2008; French et al, 2016), to seasonal (Huang et al., 2015), and even diurnal differences post-deforestation that may impact net wildfire feedback to climate (Shultz et al., 2017). The radiative response to wildfire changes across latitudinal gradients (Jin et al., 2012), and between local and global scales (Ward et al., 2012; Liu et al., 2019). Additionally, the original vegetation type burned influences aspects of wildfire's impact on climate such as the original albedo (French et al., 2016), likely fire severity and intensity (Rogers et al 2015), and time to pre-fire ecosystem recovery (French et al., 2016) or alternate ecosystem establishment (Johnstone et al., 2010b). The mechanisms that appear to have the largest effect include carbon release and sequestration (e.g. Harrison et al. 2018), changes in surface albedo (e.g. Huang et al. 2015), altered evapotranspiration (Liu et al 2019), and aerosol effects both directly and also indirectly via cloud processes (e.g. Stone et al., 2008; Zhang et al., 2017). Wildfires' potential role as a feedback to climate in the mi-Pliocene Arctic is suggested by its prevalence through this >20000 year sequence, the impact of forest fire in modern ecosystems, and preliminary modelling of the complex direct impacts on the surface radiative budget (e.g. short term black carbon deposition on snow and ice and long-term changes in albedo) and direct and indirect effects on the top of the atmosphere radiative budget (i.e. aerosol emissions; Feng et al., 2016). Further

352 modelling experiments are needed to determine if wildfire played a significant role in the magnitude and seasonal
353 patterns of mid-Pliocene arctic amplification of temperature.
354 An increase in atmospheric convection has been simulated in response to diminished sea-ice during warmer intervals
355 (Abbot and Tziperman, 2008), but this study did not confirm if this increase in atmospheric convection was sufficient
356 to cause lightning ignitions. An alternative ignition source for combustion of biomass on Ellesmere Island during the
357 Pliocene is coal seam fires, which have been documented to be burning at this time (Estrada et al., 2009). However,
358 given the interaction of summer warmth and ignition by lightning within the same climate range as posited for BP, we
359 consider lightning the most likely source of ignition for Pliocene fires in the High Arctic.
360 Fire return intervals cannot be calculated from the BP charcoal counts due to the absence of a satisfactory age-depth
361 model and discontinuous sampling. As strong interactions are observed between fire regime and ecosystem
362 assemblage in the boreal forest (Brown and Giesecke, 2014; Kasischke and Turetsky, 2006), and in response to
363 climate, comparison with modern fire regimes for areas with shared species compositions and climates may inform a
364 potential range of mean fire return interval (MFRI).
365 Matthews and Fyles (2000) indicated that the Pliocene BP environment was characterized by an open larch
366 dominated forest-tundra environment, sharing most species in common with those now found in three regions,
367 including central Alaska to Washington in western North America, the region centered around the Canadian/US border
368 in eastern North America, as well as Fennoscandia in Europe. The modern area with the most species in common with
369 BP is central northern Alaska (Fig. 7A). The area over which shared species were calculated is largely tundra, but
370 includes the ecotone between tundra and boreal forest. Other zones that share many species with BP are continuous
371 with Alaska down the western coast of North America to the region around the border of Canada and the United States,
372 the eastern coast of North America in the region around the border of Canada and the United States (~50°N), and
373 central Fennoscandia. Of these zones, the MST of Alaskan tundra sites (6–9°C) are less similar to BP (15.4°C) than
374 ~50°N on both western and eastern coastal North American sites and central Fennoscandia (12–18°C, Fig. 7B). The
375 eastern coast of North America has higher rainfall during the summer (>270 mm), than the west coast and Alaska
376 (Fig. 7C), which correlates to the timing of western fires. The low summer precipitation for much of the west (<200
377 mm), is consistent with previously published summer precipitation estimates for BP (~190 mm). As a result, the fire
378 regime of the west coast ~50°N may be a better analogue for BP than the east coast of North America. In central
379 Fennoscandia there is also a west vs. east coastal variation in summer precipitation with the western, Nordic part of
380 the region experiencing higher summer precipitation (252– >288 mm), than the more similar eastern, Swedish part of
381 the region (~198 mm).
382 Investigation of the modern fire detection data (Fig. 7D) suggests that the two regions most climatically similar to
383 BP, ~50°N western North America and central Sweden, have radically different fire regimes. It is likely this is caused
384 by historical fire suppression in Sweden that limits the utility of modern data for comparison with this study (Brown
385 and Giesecke, 2014; Niklasson and Granström, 2004). To understand the fire regimes, as shaped by climate and species
386 composition rather than human impacts, we considered both the modern and recent Holocene reconstructions for these
387 regions (Table 1). This shows that, a) within any region variation arises from the complex spatial patterning of fire
388 across landscapes, and b) that the regions most similar to BP (~50°N western North American and eastern

Fennoscandian reconstructions for the recent Holocene) have shorter fire return intervals than the cooler Alaskan tundra or wetter summer ~50°N region of the eastern North American coast.

While the shared species for Siberia appears low, the total number of observations for Siberia in the modern biodiversity database used is likewise low – and the latter is a potential cause of the former. Given the similar climate to BP on the Central Siberian Plateau and some key aspects of the floras in Siberia such as the dominance of larch, we considered the fire regime of the larch forests of Siberia. Kharuk et al. (2016; 2011) studied MFRIs across Siberia, from 64°N to 71°N, the northern limit of larch stands. They found an average MFRI across that range of 110 years, with MFRI increasing from 80 years in the southern latitudes to ~300 in the north (Table 1). Based on similarity of the climate variables, the more southerly MFRIs (~80 years) may be a better analogue. Key differences between boreal fires in North America compared to Russia are a higher fire frequency with more burned area in Russia, but a much lower crown fire and a difference in timing of disturbance, with spring fires prevailing in Russia compared to mid-summer fires in western Canada (de Groot et al., 2013; Rogers et al., 2015).

The pollen-based vegetation reconstruction derived in this study indicates that open *Larix-Betula* parkland persisted in the basal (380.3-380.4 MASL) parts of the sequence. Groundcover was additionally dominated by shrub birch, ericaceous heath and ferns. While the regional climate may have been somewhat dry, the record suggests that, locally, a moist fen environment dominated by Cyperaceae, existed near the sampling location. Shrubs including *Alnus* and *Salix* likely occupied the wetland margins.

The corresponding relatively low concentration of charcoal in this stratigraphic interval may reflect lower severity fires or higher sedimentation rates. We consider the former more likely due to the depositional environment of Unit III from Mitchell et al. 2016, a lake edge fen peat in a beaver pond or small lake, without evidence of high sediment influx overwhelming peat production. We posit that a surface fire regime, somewhat like that in southern central Siberia existed. This premise is also supported by the fire ecology characteristics of the dominant vegetation. *Larix* does not support crown fires due to leaf moisture content (de Groot et al., 2013) and self-pruning (Kobayashi et al., 2007). The persistence and success of larch in modern-day Siberia appears to be driven by its high growth rate (Jacquelyn et al., 2017), tolerance of frequent surface fire due to thick lower bark (Kobayashi et al., 2007), and tolerance of spring drought due to its deciduous habit (Berg and Chapin III, 1994). Arboreal *Betula* are very intolerant of fire and easily girdled. However, they are quick to resprout and are often found in areas with short fire return intervals. Like *Larix*, arboreal *Betula* have high moisture content of their foliage and are not prone to crown fires. *Betula* nana L., an extant dwarf birch, is a fire endurer that resprouts from underground rhizomes or roots (Racine et al., 1987) thus regenerating quickly following lower severity fires (de Groot et al., 1997). The vegetation and fire regime characteristics are similar further up the sequence at 381.10-381.25 MASL, with the exception that ferns increased in abundance while heath decreased.

In the upper part of the sequence (381.35-381.45 MASL), where charcoal was abundant, the *Larix-Betula* parkland was replaced by a mixed boreal forest assemblage with a fern understory. Canopy cover was more closed compared to the preceding intervals. The forest was dominated by *Larix* and *Picea*, with lesser amounts of *Pinus*. While *Betula* remained part of the forest, it decreased in abundance possibly due to increased competition with the conifers. Based on exploratory CRACLE analyses of climate preferences using GBIF occurrence data (GBIF.org, 2018a, b, c, d) of

426 the dominant taxa (*Larix-Betula* vs. *Larix-Picea-Pinus*), the expansion of conifers could indicate slightly warmer
427 summers (MST ~15.8 ºC vs. 17.1 ºC). This result differs from the stable MST estimated by bacterial tetraethers,
428 although within reported error, and the small change is certainly within the climate distributions of both communities.
429 The CRACLE analyses also suggest that slightly drier conditions may have prevailed during the three wettest months
430 (249-285mm vs. 192-219mm). While the interaction between climate, vegetation and fire is complex, small changes
431 in MST and precipitation could have directly altered both the vegetation and fire regime, which in turn further
432 promoted fire adapted taxa. In addition to regional climatic factors, community change at the site may have been
433 further influenced by local hydrological conditions, such as channel migration, pond infilling and ecosystem
434 engineering by beaver (*Dipoides sp.*).
435 The high charcoal content of the upper portion (~ Unit IV) of the sequence has three potential explanations:
436 reworking of previously deposited charcoal, decreased sedimentation, or increased wildfire production of charcoal.
437 The first explanation seems unlikely because there is no difference in the shape of the macrocharcoal between the
438 upper and lower portions of the sequence. A change in the dimensions of the charcoal would be expected if it had
439 undergone additional physical breakdown from reworking (see Fig. S4). The second, decreased sedimentation, may
440 occur if the deposition is a result of infrequent, episodic flooding intermixed with long periods during which charcoal
441 was deposited. The recorded sedimentology does not support this explanation, but due to the complexity of flooding
442 processes, also does not disprove this explanation. The third explanation, that increased charcoal reflects increased
443 wildfire, is supported by the change in plant composition and suggests that frequent, mixed severity fires may have
444 persisted at this time. While *Larix* is associated with surface fire, *Picea* and *Pinus* are adapted to higher intensity
445 crown fires. A crown fire regime may have established as conifers expanded, altering fuel loads and flammability. For
446 example, black spruce sheds highly flammable needles, its lower branches can act as fuel ladders facilitating crown
447 fires (Kasischke et al., 2008), and black spruce was previously tentatively identified at BP (Fletcher et al., 2017).
448 While it has thin bark and shallow roots maladapted to survive fire (Auclair, 1985; Brown, 2008; Kasischke et al.,
449 2008), it releases large numbers of seeds from semi-serotinous cones, leading to rapid re-establishment (Côté et al.,
450 2003). The documentation of Onagraceae pollen at the top of the sequence could potentially reflect post-fire
451 succession. For example, the species *Epilobium angustifolium* L. is an early-seral colonizer of disturbed (i.e. burned)
452 sites, pollinated by insects.
453 It appears that the *Larix-Betula* parkland dominated intervals correspond to the peat- and sand-stratigraphic Units II
454 and III described by Mitchell et al. (2016), whereas the mixed boreal forest in the upper part of the sequence is
455 contemporaneous with Unit IV, described as peat and peaty sand, coarsening upwards. Thus, while vegetation and
456 fire regimes seemingly changed through time at this Arctic site, temperatures appear more stable, or at least to have
457 no apparent trend within analytical and reconstruction uncertainty. Thus, it is suggested that the fire regime at BP was
458 primarily regulated by regional climate and vegetation, and perhaps additionally by changing local hydrological
459 conditions. Regarding climate, MST remained high enough (> ~13.5ºC) throughout the sequence to allow for fire
460 disturbance and the pollen suggests that temperatures may have marginally increased in the upper part of the sequence.
461 Alternatively, other climate variables, such as the precipitation regime, or local hydrological change may have initiated
462 the change in vegetation community. Up-sequence changes in vegetation undoubtedly influenced fine fuel loads (e.g.

surface layer needles, mosses, and twigs) and flammability. Indeed, the fire ecological characteristics of the vegetation are consistent with a regional surface fire regime yielding to a crown fire regime.

*Betula* and *Alnus*, which occurred earlier in the depositional sequence, are favored by beaver in foraging (Busher, 1996; Haarberg and Rosell, 2006; Jenkins, 1979). Moreover, the presence of sticks cut by beaver in Unit III reveals that beavers were indeed at the site, moistening the local land surface. The lack of beaver cut sticks and changes in sediment in Unit IV may indicate that the beavers abandoned the site, possibly in response to changes in vegetation (i.e. increased conifers and decreased *Betula*) limiting preferred forage or due to lateral channel migration, as evidenced by the coarsening upward sequence described by Mitchell et al. (2016). As a result, the local land surface may have become somewhat drier, contemporaneous with the change towards *Larix-Picea-Pinus* forest and a mixed severity fire regime.

## 5. CONCLUSION

The novel temperature estimates presented here confirm that Ellesmere Island summer temperatures were considerably warmer (15.4 ± 0.8 °C) during the likely >20000-year mid-Pliocene interval (3.9 +1.5/-0.5 Ma) investigated, compared to the modern Arctic. The ~11°C higher than present day summer temperatures at Beaver Pond support an increasing effect of arctic amplification of temperatures when $CO_2$ reaches and exceeds modern levels. Our reconstruction of the paleovegetation and ecology of this unique site on Ellesmere Island suggests an assemblage similar to forests of the western margins of North America and eastern Fennoscandia. The evidence of recurrent fire and concurrent changes in taxonomic composition are indicators that fire played an active role in mid-Pliocene Arctic forests, shaping the environment as it does in the boreal forest today. Evidence from fire in the modern boreal forest suggests that fire may have had direct and indirect impacts on Earth's radiative budget at high latitudes during the Pliocene, acting as a feedback to Pliocene climate. The net impact of the component process remains unknown and modelling experiments are needed to quantitatively investigate the effects of the kind of fire regime presented here, on the Pliocene High Arctic. Collectively, these reconstructions provide new insights into the paleoclimatology and paleoecology of the Canadian High Arctic, ~3.9 Ma.

*Data Availability.* The data generated and used in this analysis are available in the supplemental information associated with this article.

*Sample Availability.* Samples used in this analysis are curated by the Canadian Museum of Nature. Sample numbers used for each analysis are given in the supplemental information (Table S3 and S4).

*Supplemental Link.* To be provided by Copernicus Publishing

*Author Contribution.* Conceptualization: A.P.B. with modification by other authors; Methodology: J.G., J.S.S.D., K.J.B., T.F.; Formal analysis: All authors; Investigation: A.P.B., J.G., K.J.B., L.W., T.F.; Resources: A.P.B., J.G., J.S.S.D., K.J.B.; Data curation: A.P.B., J.G., K.J.B., L.W., T.F.; Writing—Original draft: All authors; Writing—

Review and editing: All authors; Supervision: A.P.B., J.S.S.D., K.J.B., N.R.; Project administration: A.P.B., N.R., T.F.; Funding acquisition: A.P.B., J.G., J.S.S.D., K.J.B., N.R., T.F. (Definitions as per the CRediT Taxonomy)

*Competing interests.* The authors declare that they have no conflict of interest

*Acknowledgements.* This work was funded by NSF Polar Programs to A.P.B.; National Geographic Committee for Research and Exploration Grant (9912-16) and Endeavour Research Fellowship (5928-2017) to T.F.; National Geographic Explorer Grant (7902-05), NSERC Discovery Grant (312193), and The W. Garfield Weston Foundation grant to N.R.; student travel (N.R. supervised) was supported by the Northern Scientific Training Program (NSTP) from the government of Canada; an NSERC Discovery Grant (239961) with Northern Supplement (362148) to J.C.G; Natural Resources Canada (SO-03 PA 3.1 Forest Disturbances Wildland Fire) to K.J.B.; the European Research Council under the European Union's Seventh Framework Programme (FP7/2007-2013) / ERC grant agreement n° (226600), and funding from the Netherlands Earth System Science Center (NESSC) through a gravitation grant (NWO 024.002.001) from the Dutch Ministry for Education, Culture and Science to J.S.S.D.

We are also grateful to Nicholas Conder (Canadian Forest Service) who assisted with sample preparation for the vegetation/fire reconstruction. We also acknowledge the 2006, 2008, 2010 and 2012 field teams including D. Finney (Environment Canada), H. Larson (McGill University), M. Vavrek (McGill University), A. Dececchi (McGill University), W.T. Mitchell (Carleton University), R. Smith (University of Saskatchewan), and C. Schröder-Adams (Carleton University). The field research was supported by a paleontology permit from the Government of Nunavut, CLEY (D.R. Stenton, J. Ross) and with the permission of Qikiqtani Inuit Association, especially Grise Fiord (Nunavut). Logistic support was provided by the Polar Continental Shelf Program (M. Bergmann, B. Hyrcyk, B. Hough, M. Kristjanson, T. McConaghy, J. MacGregor and the PCSP team) and in-kind financial support through PCSP-616-16 was greatly appreciated.

## References

Abbot, D. S. and Tziperman, E.: Sea ice, high-latitude convection, and equable climates, Geophysical Research Letters, 35, 2008.

Auclair, A. N.: Postfire regeneration of plant and soil organic pools in a *Picea mariana–Cladonia stellaris* ecosystem, Canadian Journal of Forest Research, 15, 279–291, 1985.

Ballantyne, A. P., Axford, Y., Miller, G. H., Otto-Bliesner, B. L., Rosenbloom, N., and White, J. W.: The amplification of Arctic terrestrial surface temperatures by reduced sea-ice extent during the Pliocene, Palaeogeography, Palaeoclimatology, Palaeoecology, 386, 59–67, 2013.

Ballantyne, A. P., Greenwood, D. R., Sinninghe Damsté, J. S., Csank, A. Z., Eberle, J. J., and Rybczynski, N.: Significantly warmer Arctic surface temperatures during the Pliocene indicated by multiple independent proxies, Geology, 38, 603–606, 2010.

Ballantyne, A. P., Rybczynski, N., Baker, P. A., Harington, C. R., and White, D.: Pliocene Arctic temperature constraints from the growth rings and isotopic composition of fossil larch, Palaeogeography, Palaeoclimatology, Palaeoecology, 242, 188–200, 2006.

Bendle, J. A., Weijers, J. W., Maslin, M. A., Sinninghe Damsté, J. S., Schouten, S., Hopmans, E. C., Boot, C. S., and Pancost, R. D.: Major changes in glacial and Holocene terrestrial temperatures and sources of organic carbon recorded in the Amazon fan by tetraether lipids, Geochemistry, Geophysics, Geosystems, 11, 2010.

Berg, E. E. and Chapin III, F. S.: Needle loss as a mechanism of winter drought avoidance in boreal conifers, Canadian Journal of Forest Research, 24, 1144–1148, 1994.

Bergeron, Y.: The influence of island and mainland lakeshore landscapes on boreal forest fire regimes, Ecology, 72, 1980–1992, 1991.

Bergeron, Y., Cyr, D., Drever, C. R., Flannigan, M., Gauthier, S., Kneeshaw, D., Lauzon, È., Leduc, A., Goff, H. L., Lesieur, D., and Logan, K.: Past, current, and future fire frequencies in Quebec's commercial forests: implications for the cumulative effects of harvesting and fire on age-class structure and natural disturbance-based management, Canadian Journal of Forest Research, 36, 2737–2744, 2006.

Bonan, G., B.: Forests and Climate Change: Forcings, Feedbacks, and the Climate Benefits of Forests, Science, 320, 1444–1449, 2008.

Bouchard, M., Pothier, D., and Gauthier, S.: Fire return intervals and tree species succession in the North Shore region of eastern Quebec, Canadian Journal of Forest Research, 38, 1621–1633, 2008.

Brigham-Grette, J. and Carter, L. D.: Pliocene Marine Transgressions of Northern Alaska: Circumarctic Correlations and Paleoclimatic Interpretations, Arctic, 45, 74–89, 1992.

Brown, K. J. and Giesecke, T.: Holocene fire disturbance in the boreal forest of central Sweden, Boreas, 43, 639–651, 2014.

Brown, K. J. and Power, M. J.: Charred particle analyses. In: Encyclopedia of Quaternary Science, Elias, S. (Ed.), Elsevier, Amsterdam, 2013.

Brown, M.: Fire and Ice: Fire Severity and Future Flammability in Alaskan Black Spruce Forests, Fire Science Brief, 2008. 1–6, 2008.

Bush, E. and Lemmen, D.S.(eds): Canada's Changing Climate Report; Government of Canada, Ottawa, ON. 444 p., 2019

Busher, P. E.: Food Caching Behavior of Beavers (*Castor canadensis*): Selection and Use of Woody Species, The American Midland Naturalist, 135, 343-348, 1996.

Clymo, R. S.: The Origin of Acidity in Sphagnum Bogs, The Bryologist, 67, 427–431, 1964.

Côté, M., Ferron, J., and Gagnon, R.: Impact of seed and seedling predation by small rodents on early regeneration establishment of black spruce, Canadian Journal of Forest Research, 33, 2362–2371, 2003.

Csank, A. Z., Patterson, W. P., Eglington, B. M., Rybczynski, N., and Basinger, J. F.: Climate variability in the Early Pliocene Arctic: Annually resolved evidence from stable isotope values of sub-fossil wood, Ellesmere Island, Canada, Palaeogeography, Palaeoclimatology, Palaeoecology, 308, 339–349, 2011a.

Csank, A. Z., Tripati, A. K., Patterson, W. P., Eagle, R. A., Rybczynski, N., Ballantyne, A. P., and Eiler, J. M.: Estimates of Arctic land surface temperatures during the early Pliocene from two novel proxies, Earth and Planetary Science Letters, 304, 291–299, 2011b.

de Groot, W. J., Cantin, A. S., Flannigan, M. D., Soja, A. J., Gowman, L. M., and Newbery, A.: A comparison of Canadian and Russian boreal forest fire regimes, Forest Ecology and Management, 294, 23–34, 2013.

de Groot, W. J., Thomas, P. A., and Wein, R. W.: *Betula nana* L. *and Betula glandulosa* Michx, Journal of Ecology, 85, 241–264, 1997.

De Jonge, C., Hopmans, E. C., Stadnitskaia, A., Rijpstra, W. I. C., Hofland, R., Tegelaar, E., and Sinninghe Damsté, J. S.: Identification of novel penta-and hexamethylated branched glycerol dialkyl glycerol tetraethers in peat using HPLC–MS 2, GC–MS and GC–SMB-MS, Organic geochemistry, 54, 78–82, 2013.

De Jonge, C., Hopmans, E. C., Zell, C. I., Kim, J.-H., Schouten, S., and Sinninghe Damsté, J. S.: Occurrence and abundance of 6-methyl branched glycerol dialkyl glycerol tetraethers in soils: Implications for palaeoclimate reconstruction, Geochimica et Cosmochimica Acta, 141, 97–112, 2014.

De Jonge, C., Stadnitskaia, A., Hopmans, E. C., Cherkashov, G., Fedotov, A., Streletskaya, I. D., Vasiliev, A. A., and Sinninghe Damsté, J. S.: Drastic changes in the distribution of branched tetraether lipids in suspended matter and sediments from the Yenisei River and Kara Sea (Siberia): Implications for the use of brGDGT-based proxies in coastal marine sediments, Geochimica et Cosmochimica Acta, 165, 200–225, 2015.

de Lafontaine, G. and Payette, S.: Shifting zonal patterns of the southern boreal forest in eastern Canada associated with changing fire regime during the Holocene, Quaternary Science Reviews, 30, 867–875, 2011.

Dowsett, H., Dolan, A., Rowley, D., Pound, M., Salzmann, U., Robinson, M., Chandler, M., Foley, K., and Haywood, A.: The PRISM4 (mid-Piacenzian) palaeoenvironmental reconstruction, Climate of the Past, doi: doi:10.5194/cp-12-1519-2016, 2016. 2016.

Estrada, S., Piepjohn, K., Frey, M. J., Reinhardt, L., Andruleit, H., and von Gosen, W.: Pliocene coal-seam fires on southern Ellesmere Island, Canadian Arctic, Neues Jahrbuch für Geologie und Paläontologie - Abhandlungen, 251, 33-52, 2009.

Feng, R., Otto-Bliesner, B., Fletcher, T., Ballantyne, A., and Brady, E.: Contributions to Pliocene Arctic warmth from removal of anthropogenic aerosol and enhanced forest fire emissions, San Francisco, USA. 2016, PP33A-2344.

Feng, R., Otto-Bliesner, B. L., Fletcher, T. L., Tabor, C. R., Ballantyne, A. P., and Brady, E. C.: Amplified Late Pliocene terrestrial warmth in northern high latitudes from greater radiative forcing and closed Arctic Ocean gateways, Earth and Planetary Science Letters, 466, 129-138, 2017.

Flannigan, M., Stocks, B., Turetsky, M., and Wotton, M.: Impacts of climate change on fire activity and fire management in the circumboreal forest, Global Change Biology, 15, 549–560, 2009.

Fletcher, T., Feng, R., Telka, A. M., Matthews, J. V., and Ballantyne, A.: Floral dissimilarity and the influence of climate in the Pliocene High Arctic: Biotic and abiotic influences on five sites on the Canadian Arctic Archipelago, Frontiers in Ecology and Evolution, 5, 19, 2017.

Foster, L. C., Pearson, E. J., Juggins, S., Hodgson, D. A., Saunders, K. M., Verleyen, E., and Roberts, S. J.: Development of a regional glycerol dialkyl glycerol tetraether (GDGT)–temperature calibration for Antarctic and sub-Antarctic lakes, Earth and Planetary Science Letters, 433, 370–379, 2016.

Francis, J. and Skific, N.: Evidence linking rapid Arctic warming to mid-latitude weather patterns, Philosophical Transactions of the Royal Society A: Mathematical, Physical and Engineering Sciences, 373, 1–12, 2015.

French, N. H., Whitley, M. A., and Jenkins, L. K.: Fire disturbance effects on land surface albedo in Alaskan tundra, Journal of Geophysical Research: Biogeosciences, 121, 841–854, 2016.

GBIF.org: GBIF Occurrence Download (Beaver Pond extant species) http://doi.org/10.15468/dl.ertiqj 1st February 2017.

GBIF.org: GBIF Occurrence Download (*Betula*) https://doi.org/10.15468/dl.akxgp5 11th May 2018a.

GBIF.org: GBIF Occurrence Download (*Larix*) https://doi.org/10.15468/dl.mfhnci 11th May 2018b.

GBIF.org: GBIF Occurrence Download (*Picea*) https://doi.org/10.15468/dl.wi7jdc 11th May 2018c.

GBIF.org: GBIF Occurrence Download (*Pinus*) https://doi.org/10.15468/dl.vwfjj2 11th May 2018d.

Greene, G. A. and Daniels, L. D.: Spatial interpolation and mean fire interval analyses quantify historical mixed-severity fire regimes, International Journal of Wildland Fire, 26, 136–147, 2017.

Haarberg, O. and Rosell, F.: Selective foraging on woody plant species by the Eurasian beaver (*Castor fiber*) in Telemark, Norway, Journal of Zoology, 270, 201-208, 2006.

Harrison, S., Bartlein, P. J., Brovkin, V., Houweling, S., Kloster, S., and Prentice, I. C.: The biomass burning contribution to climate-carbon-cycle feedback, Earth System Dynamics, 9, 663–677, 2018.

Huang, S., Dahal, D., Liu, H., Jin, S., Young, C., Li, S., and Liu, S.: Spatiotemporal variation of surface shortwave forcing from fire-induced albedo change in interior Alaska, Canadian Journal of Forest Research, 45, 276-285, 2014.

Haywood, A. M., Dowsett, H. J., and Dolan, A. M.: Integrating geological archives and climate models for the mid-Pliocene warm period, Nature communications, 7, 1-14, 2016.

Higuera, P., Barnes, J. L., Chipman, M. L., Urban, M., and Hu, F. S.: The burning tundra: A look back at the last 6,000 years of fire in the Noatak National Preserve, Northwestern Alaska, Alaska Park Science, 10, 37–41, 2011.

Higuera, P. E., Brubaker, L. B., Anderson, P. M., Hu, F. S., and Brown, T. A.: Vegetation mediated the impacts of postglacial climate change on fire regimes in the south-central Brooks Range, Alaska, Ecological Monographs, 79, 201–219, 2009.

Hijmans, R. J., Cameron, S. E., Parra, J. L., Jones, P. G., and Jarvis, A.: Very high resolution interpolated climate surfaces for global land areas, International Journal of Climatology, 25, 1965–1978, 2005.

Hopmans, E. C., Schouten, S., and Sinninghe Damsté, J. S.: The effect of improved chromatography on GDGT-based palaeoproxies, Organic Geochemistry, 93, 1–6, 2016.

Hu, F. S., Higuera, P. E., Walsh, J. E., Chapman, W. L., Duffy, P. A., Brubaker, L. B., and Chipman, M. L.: Tundra burning in Alaska: Linkages to climatic change and sea ice retreat, Journal of Geophysical Research: Biogeosciences, 115, 2010.

639 Huguet, C., Hopmans, E. C., Febo-Ayala, W., Thompson, D. H., Sinninghe Damsté, J. S., and Schouten, S.: An
640 improved method to determine the absolute abundance of glycerol dibiphytanyl glycerol tetraether lipids, Organic
641 Geochemistry, 37, 1036–1041, 2006.
642 Hwang, Y. T., Frierson, D. M., and Kay, J. E.: Coupling between Arctic feedbacks and changes in poleward energy
643 transport, Geophysical Research Letters, 38, 2011.
644 Jacquelyn, K. S., Adrianna, C. F., Herman, H. S., Amanda, H.-H., Alexander, K., Tatiana, L., Dmitry, E., and Elena,
645 S.: Fire disturbance and climate change: implications for Russian forests, Environmental Research Letters, 12, 035003,
646 2017.
647 Jenkins, S. H.: Seasonal and year-to-year differences in food selection by beavers, Oecologia, 44, 112-116, 1979.
648 Jin, Y., Randerson, J. T., Goulden, M. L., and Goetz, S. J.: Post-fire changes in net shortwave radiation along a
649 latitudinal gradient in boreal North America, Geophysical Research Letters, 39, L13403, 2012.
650 Johnstone, J. F., Chapin, F. S., Hollingsworth, T. N., Mack, M. C., Romanovsky, V., and Turetsky, M.: Fire, climate
651 change, and forest resilience in interior Alaska, Canadian Journal of Forest Research, 40, 1302–1312, 2010a.
652 Johnstone, J. F., Hollingsworth, T. N., Chapin, F. S., and Mack, M. C.: Changes in fire regime break the legacy lock
653 on successional trajectories in Alaskan boreal forest, Global Change Biology, 16, 1281–1295, 2010b.
654 Johnstone, J. F. and Kasischke, E. S.: Stand-level effects of soil burn severity on postfire regeneration in a recently
655 burned black spruce forest, Canadian Journal of Forest Research, 35, 2151–2163, 2005.
656 Jones, P. D. and Moberg, A.: Hemispheric and large-scale surface air temperature variations: An extensive revision
657 and an update to 2001, Journal of Climate, 16, 206–223, 2003.
658 Kasischke, E. S. and Turetsky, M. R.: Recent changes in the fire regime across the North American boreal region—
659 spatial and temporal patterns of burning across Canada and Alaska, Geophysical research letters, 33, 2006.
660 Kasischke, E. S., Turetsky, M. R., Ottmar, R. D., French, N. H., Hoy, E. E., and Kane, E. S.: Evaluation of the
661 composite burn index for assessing fire severity in Alaskan black spruce forests, International Journal of Wildland
662 Fire, 17, 515–526, 2008.
663 Kasischke, E. S., Williams, D., and Barry, D.: Analysis of the patterns of large fires in the boreal forest region of
664 Alaska, International Journal of Wildland Fire, 11, 131–144, 2002.
665 Kharuk, V. I., Dvinskaya, M. L., Petrov, I. A., Im, S. T., and Ranson, K. J.: Larch forests of Middle Siberia: long-term
666 trends in fire return intervals, Regional Environmental Change, doi: 10.1007/s10113-016-0964-9, 2016. 1–9, 2016.
667 Kharuk, V. I., Ranson, K. J., Dvinskaya, M. L., and Im, S. T.: Wildfires in northern Siberian larch dominated
668 communities, Environmental Research Letters, 6, 045208, 2011.
669 Kobayashi, M., Nemilostiv, Y. P., Zyryanova, O. A., Kajimoto, T., Matsuura, Y., Yoshida, T., Satoh, F., Sasa, K., and
670 Koike, T.: Regeneration after forest fires in mixed conifer broad-leaved forests of the Amur region in far eastern
671 Russia: the relationship between species specific traits against fire and recent fire regimes, Eurasian Journal of Forest
672 Research, 10, 51–58, 2007.
673 Kooijman, A. and Westhoff, V.: Variation in habitat factors and species composition of *Scorpidium scorpioides*
674 communities in NW-Europe, Plant Ecology, 117, 133–150, 1995.

675 Kooijman, A. M. and Paulissen, M. P. C. P.: Higher acidification rates in fens with phosphorus enrichment, Applied
676 Vegetation Science, 9, 205–212, 2006.
677 Lifton, N., Sato, T., and Dunai, T. J.: Scaling in situ cosmogenic nuclide production rates using analytical
678 approximations to atmospheric cosmic-ray fluxes, Earth and Planetary Science Letters, 386, 149–160, 2014.
679 Lisiecki, L. E. and Raymo, M. E.: A Plio-Pleistocene stack of 57 globally distributed benthic $\delta^{18}O$ records,
680 Paleoceanography, 20, 2005.
681 Liu, Z., Ballantyne, A. P., and Cooper, L. A.: Biophysical feedback of global forest fires on surface temperature,
682 Nature Communications, 10, 214, 2019.Loomis, S. E., Russell, J. M., Ladd, B., Street-Perrott, F. A., and Sinninghe
683 Damsté, J. S.: Calibration and application of the branched GDGT temperature proxy on East African lake sediments,
684 Earth and Planetary Science Letters, 357, 277–288, 2012.
685 Lorimer, C. G.: The Presettlement Forest and Natural Disturbance Cycle of Northeastern Maine, Ecology, 58, 139–
686 148, 1977.
687 Luthi, D., Le Floch, M., Bereiter, B., Blunier, T., Barnola, J.-M., Siegenthaler, U., Raynaud, D., Jouzel, J., Fischer,
688 H., Kawamura, K., and Stocker, T. F.: High-resolution carbon dioxide concentration record 650,000-800,000 years
689 before present, Nature, 453, 379–382, 2008.
690 Lynch, J. A., Clark, J. S., Bigelow, N. H., Edwards, M. E., and Finney, B. P.: Geographic and temporal variations in
691 fire history in boreal ecosystems of Alaska, Journal of Geophysical Research: Atmospheres, 107, FFR 8-1–FFR 8-17,
692 2002.
693 Mack, M. C., Bret-Harte, M. S., Hollingsworth, T. N., Jandt, R. R., Schuur, E. A. G., Shaver, G. R., and Verbyla, D.
694 L.: Carbon loss from an unprecedented Arctic tundra wildfire, Nature, 475, 489–492, 2011.
695 Marshall, J., Armour, K. C., Scott, J. R., Kostov, Y., Hausmann, U., Ferreira, D., Shepherd, T. G., and Bitz, C. M.:
696 The ocean's role in polar climate change: asymmetric Arctic and Antarctic responses to greenhouse gas and ozone
697 forcing, Philosophical Transactions of the Royal Society of London A: Mathematical, Physical and Engineering
698 Sciences, 372, 20130040, 2014.
699 Matthews Jr, J. V. and Ovenden, L. E.: Late Tertiary plant macrofossils from localities in Arctic/sub- Arctic North
700 America: a review of the data, Arctic, 43, 364–392, 1990.
701 Matthews, J. V. J. and Fyles, J. G.: Late Tertiary plant and arthropod fossils from the High Terrace Sediments on the
702 Fosheim Peninsula of Ellesmere Island (Northwest Territories, District of Franklin), Geological Survey of Canada,
703 Bulletin, 529, 295–317, 2000.
704 Mattson, M. D.: Acid lakes and rivers. In: Environmental Geology, Springer Netherlands, Dordrecht, 1999.
705 McAndrews, J. H., Berti, A. A., and Norris, G.: Key to the Quaternary pollen and spores of the Great Lakes region,
706 1973. 1973.
707 Miller, G. H., Alley, R. B., Brigham-Grette, J., Fitzpatrick, J. J., Polyak, L., Serreze, M. C., and White, J. W. C.: Arctic
708 amplification: can the past constrain the future?, Quaternary Science Reviews, 29, 1779–1790, 2010.
709 Mitchell, W. T., Rybczynski, N., Schröder-Adams, C., Hamilton, P. B., Smith, R., and Douglas, M.: Stratigraphic and
710 Paleoenvironmental Reconstruction of a Mid-Pliocene Fossil Site in the High Arctic (Ellesmere Island, Nunavut):
711 Evidence of an Ancient Peatland with Beaver Activity, Arctic, 69, 185–204, 2016.

712 Moore, P. D., Webb, J. A., and Collison, M. E.: Pollen analysis, Blackwell Scientific Publications, Oxford, 1991.
713 Naafs, B., Inglis, G., Zheng, Y., Amesbury, M., Biester, H., Bindler, R., Blewett, J., Burrows, M., del Castillo Torres,
714 D., and Chambers, F. M.: Introducing global peat-specific temperature and pH calibrations based on brGDGT bacterial
715 lipids, Geochimica et Cosmochimica Acta, 208, 285–301, 2017.
716 Niemann, H., Stadtnitskaia, A., Wirth, S., Gilli, A., Anselmetti, F., Sinninghe Damsté, J., Schouten, S., Hopmans, E.,
717 and Lehmann, M.: Bacterial GDGTs in Holocene sediments and catchment soils of a high Alpine lake: application of
718 the MBT/CBT-paleothermometer, Climate of the Past, 8, 889-906, 2012.
719 Niklasson, M. and Drakenberg, B.: A 600-year tree-ring fire history from Norra Kvills National Park, southern
720 Sweden: implications for conservation strategies in the hemiboreal zone, Biological Conservation, 101, 63–71, 2001.
721 Niklasson, M. and Granström, A.: Fire in Sweden – History, Research, Prescribed Burning and Forest Certification,
722 International Forest Fire News, 30, 80–83, 2004.
723 Niklasson, M. and Granström, A.: Numbers and sizes of fires: Long-term spatially explicit fire history in a Swedish
724 boreal landscape, Ecology, 81, 1484–1499, 2000.
725 Otto-Bliesner, B. L. and Upchurch Jr, G. R.: Vegetation-induced warming of high-latitude regions during the Late
726 Cretaceous period, Nature, 385, 804, 1997.
727 Pagani, M., Liu, Z., LaRiviere, J., and Ravelo, A. C.: High Earth-system climate sensitivity determined from Pliocene
728 carbon dioxide concentrations, Nature Geoscience, 3, 27–30, 2010.
729 Pearson, E. J., Juggins, S., Talbot, H. M., Weckström, J., Rosén, P., Ryves, D. B., Roberts, S. J., and Schmidt, R.: A
730 lacustrine GDGT-temperature calibration from the Scandinavian Arctic to Antarctic: Renewed potential for the
731 application of GDGT-paleothermometry in lakes, Geochimica et Cosmochimica Acta, 75, 6225–6238, 2011.
732 Peterse, F., Prins, M. A., Beets, C. J., Troelstra, S. R., Zheng, H., Gu, Z., Schouten, S., and Sinninghe Damsté, J. S.:
733 Decoupled warming and monsoon precipitation in East Asia over the last deglaciation, Earth and Planetary Science
734 Letters, 301, 256–264, 2011.
735 Powers, L. A., Werne, J. P., Johnson, T. C., Hopmans, E. C., Sinninghe Damsté, J. S., and Schouten, S.: Crenarchaeotal
736 membrane lipids in lake sediments: A new paleotemperature proxy for continental paleoclimate reconstruction?,
737 Geology, 32, 613–616, 2004.
738 R Core Team: R: A language and environment for statistical computing. R Foundation for Statistical Computing,
739 Vienna, Austria, 2016.
740 Racine, C. H., Johnson, L. A., and Viereck, L. A.: Patterns of Vegetation Recovery after Tundra Fires in Northwestern
741 Alaska, U.S.A, Arctic and Alpine Research, 19, 461–469, 1987.
742 Randerson, J., Liu, H., Flanner, M., Chambers, S., Jin, Y., Hess, P., Pfister, G., Mack, M., Treseder, K., and Welp, L.:
743 The impact of boreal forest fire on climate warming, Science, 314, 1130–1132, 2006.
744 Robinson, M. M.: New Quantitative Evidence of Extreme Warmth in the Pliocene Arctic, Stratigraphy, 6, 265–275,
745 2009.
746 Rogers, B. M., Soja, A. J., Goulden, M. L., and Randerson, J. T.: Influence of tree species on continental differences
747 in boreal fires and climate feedbacks, Nature Geoscience, 8, 228–234, 2015.

748 Royer, D. L., Berner, R. A., and Park, J.: Climate sensitivity constrained by $CO_2$ concentrations over the past 420
749 million years, Nature, 446, 530-532, 2007.
750 Russell, J. M., Hopmans, E. C., Loomis, S. E., Liang, J., and Sinninghe Damsté, J. S.: Distributions of 5- and 6-methyl
751 branched glycerol dialkyl glycerol tetraethers (brGDGTs) in East African lake sediment: Effects of temperature, pH,
752 and new lacustrine paleotemperature calibrations, Geochimica et Cosmochimica Acta, 117, 56–69, 2018.
753 Ryan, K. C.: Dynamic interactions between forest structure and fire behavior in boreal ecosystems, Silva Fennica, 36,
754 13–39, 2002.
755 Rybczynski, N., Gosse, J. C., Richard Harington, C., Wogelius, R. A., Hidy, A. J., and Buckley, M.: Mid-Pliocene
756 warm-period deposits in the High Arctic yield insight into camel evolution, Nature Communications, 4, 1–9, 2013.
757 Salzmann, U., Haywood, A. M., Lunt, D., Valdes, P., and Hill, D.: A new global biome reconstruction and data-model
758 comparison for the middle Pliocene, Global Ecology and Biogeography, 17, 432–447, 2008.
759 Schultz, N. M., Lawrence, P. J., and Lee, X.: Global satellite data highlights the diurnal asymmetry of the surface
760 temperature response to deforestation, Journal of Geophysical Research: Biogeosciences, 122, 903–917, 2017.
761 Sinninghe Damsté, J. S.: Spatial heterogeneity of sources of branched tetraethers in shelf systems: The geochemistry
762 of tetraethers in the Berau River delta (Kalimantan, Indonesia), Geochimica et Cosmochimica Acta, 186, 13–31, 2016.
763 Sinninghe Damsté J.S., Rijpstra W.I.C., Foesel B.U., Huber K., Overmann J., Nakagawa S., Joong Jae Kim, Dunfield
764 P.F. Dedysh S.N., Villanueva L. (2018) An overview of the occurrence of ether- and ester-linked iso-diabolic acid
765 membrane lipids in microbial cultures of the Acidobacteria: Implications for brGDGT palaeoproxies for temperature
766 and pH. Organic Geochemistry, 124, 63–76.
767 Sinninghe Damsté, J. S., Rijpstra, W. I. C., Hopmans, E. C., Foesel, B. U., Wüst, P. K., Overmann, J., Tank, M.,
768 Bryant, D. A., Dunfield, P. F., Houghton, K., and Stott, M. B.: Ether- and Ester-Bound iso-Diabolic Acid and Other
769 Lipids in Members of Acidobacteria Subdivision 4, Applied and Environmental Microbiology, 80, 5207–5218, 2014.
770 Sinninghe Damsté, J. S., Rijpstra, W. I. C., Hopmans, E. C., Weijers, J. W., Foesel, B. U., Overmann, J., and Dedysh,
771 S. N.: 13, 16-Dimethyl octacosanedioic acid (iso-diabolic acid), a common membrane-spanning lipid of Acidobacteria
772 subdivisions 1 and 3, Applied and Environmental Microbiology, 77, 4147–4154, 2011.
773 Stap, L. B., de Boer, B., Ziegler, M., Bintanja, R., Lourens, L. J., and van de Wal, R. S.: $CO_2$ over the past 5 million
774 years: Continuous simulation and new $\delta$11B-based proxy data, Earth and Planetary Science Letters, 439, 1–10, 2016.
775 Stone, R., Anderson, G., Shettle, E., Andrews, E., Loukachine, K., Dutton, E., Schaaf, C., and Roman, M.: Radiative
776 impact of boreal smoke in the Arctic: Observed and modeled, Journal of Geophysical Research: Atmospheres, 113,
777 2008.
778 Swann, A. L., Fung, I. Y., Levis, S., Bonan, G. B., and Doney, S. C.: Changes in Arctic vegetation amplify high-
779 latitude warming through the greenhouse effect, Proceedings of the National Academy of Sciences of the United States
780 of America, 107, 1295-1300, 2010.
781 Tedford, R. H. and Harington, C. R.: An Arctic mammal fauna from the early Pliocene of North America, Nature,
782 425, 388–390, 2003.
783 Van Wagner, C. E., Finney, M. A., and Heathcott, M.: Historical fire cycles in the Canadian Rocky Mountain parks,
784 Forest Science, 52, 704-717, 2006.

785 Wang, X., Rybczynski, N., Harington, C. R., White, S. C., and Tedford, R. H.: A basal ursine bear (*Protarctos*
786 *abstrusus*) from the Pliocene High Arctic reveals Eurasian affinities and a diet rich in fermentable sugars, Scientific
787 reports, 7, 17722, 2017.
788 Ward, D., Kloster, S., Mahowald, N., Rogers, B., Randerson, J., and Hess, P.: The changing radiative forcing of fires:
789 global model estimates for past, present and future, Atmospheric Chemistry and Physics, 12, 10857–10886, 2012.
790 Warden, L., Jung-Hyun, K., Zell, C., Vis, G.-J., de Stigter, H., Bonnin, J., and Sinninghe Damsté, J. S.: Examining
791 the provenance of branched GDGTs in the Tagus River drainage basin and its outflow into the Atlantic Ocean over
792 the Holocene to determine their usefulness for paleoclimate applications, Biogeosciences, 13, 5719, 2016.
793 Weijers, J. W., Schefuß, E., Schouten, S., and Sinninghe Damsté, J. S.: Coupled thermal and hydrological evolution
794 of tropical Africa over the last deglaciation, Science, 315, 1701–1704, 2007a.
795 Weijers, J. W., Schouten, S., van den Donker, J. C., Hopmans, E. C., and Sinninghe Damsté, J. S.: Environmental
796 controls on bacterial tetraether membrane lipid distribution in soils, Geochimica et Cosmochimica Acta, 71, 703-713,
797 2007b.
798 Weijers, J. W. H., Schouten, S., van den Donker, J. C., Hopmans, E. C., and Sinninghe Damsté, J. S.: Environmental
799 controls on bacterial tetraether membrane lipid distribution in soils, Geochimica et Cosmochimica Acta, 71, 703-713,
800 2007c.
801 Whitman, E., Batllori, E., Parisien, M. A., Miller, C., Coop, J. D., Krawchuk, M. A., Chong, G. W., and Haire, S. L.:
802 The climate space of fire regimes in north-western North America, Journal of Biogeography, 42, 1736–1749, 2015.
803 Wright, C. S. and Agee, J. K.: Fire and vegetation history in the eastern Cascade Mountains, Washington, Ecological
804 Applications, 14, 443–459, 2004.
805 Yang, G., Zhang, C. L., Xie, S., Chen, Z., Gao, M., Ge, Z., and Yang, Z.: Microbial glycerol dialkyl glycerol tetraethers
806 from river water and soil near the Three Gorges Dam on the Yangtze River, Organic Geochemistry, 56, 40–50, 2013.
807 Yarie, J.: Forest fire cycles and life tables: a case study from interior Alaska, Canadian Journal of Forest Research,
808 11, 554–562, 1981.
809 Young, A. M., Higuera, P. E., Duffy, P. A., and Hu, F. S.: Climatic thresholds shape northern high-latitude fire regimes
810 and imply vulnerability to future climate change, Ecography, 40, 606–617, 2017.
811 Zech, R., Gao, L., Tarozo, R., and Huang, Y.: Branched glycerol dialkyl glycerol tetraethers in Pleistocene loess-
812 paleosol sequences: three case studies, Organic geochemistry, 53, 38–44, 2012.
813 Zell, C., Kim, J.-H., Moreira-Turcq, P., Abril, G., Hopmans, E. C., Bonnet, M.-P., Sobrinho, R. L., and Sinninghe
814 Damsté, J. S.: Disentangling the origins of branched tetraether lipids and crenarchaeol in the lower Amazon River:
815 Implications for GDGT-based proxies, Limnology and Oceanography, 58, 343–353, 2013.
816 Zhang, Y., Forrister, H., Liu, J., Dibb, J., Anderson, B., Schwarz, J. P., Perring, A. E., Jimenez, J. L., Campuzano-
817 Jost, P., Wang, Y., Nenes, A., and Weber, R. J.: Top-of-atmosphere radiative forcing affected by brown carbon in the
818 upper troposphere, Nature Geosci, 10, 486-489, 2017.
819 Zheng, J., Zhang, Q., Li, Q., Zhang, Q., and Cai, M.: Contribution of sea ice albedo and insulation effects to Arctic
820 amplification in the EC-Earth Pliocene simulation, Climate of the Past, 15, 291–305, 2019.

Zhu, C., Weijers, J. W., Wagner, T., Pan, J.-M., Chen, J.-F., and Pancost, R. D.: Sources and distributions of tetraether lipids in surface sediments across a large river-dominated continental margin, Organic Geochemistry, 42, 376–386, 2011.

Zink, K.-G., Vandergoes, M. J., Mangelsdorf, K., Dieffenbacher-Krall, A. C., and Schwark, L.: Application of bacterial glycerol dialkyl glycerol tetraethers (GDGTs) to develop modern and past temperature estimates from New Zealand lakes, Organic Geochemistry, 41, 1060–1066, 2010.

**Table 1. Modern and recent Holocene fire return interval reconstructions for the candidate analogous regions considered in this study.**

| Region | Modern | | Reference | Recent Holocene | | Reference |
|---|---|---|---|---|---|---|
| Alaskan Tundra | Seward Peninsula | 273* | Kasischke et al. (2002) | Up-Valley | 263 | Higuera et al. (2011) |
| | Nulato Hills | 306* | | Down-valley | 142 | |
| Alaskan Boreal | Porcupine/ Upper Yukon (Central) | ~100 | Yarie (1981) | | | |
| | Sites near Fairbanks, and Delta Junction (Central) | 70130 | Johnstone et al. (2010a); Johnstone et al. (2010b); Johnstone and Kasischke (2005) | | | |
| | Kenai Peninsula | | Lynch et al. (2002) | Interior Alaska and Kenai Peninsula | 198 ± 90 | Lynch et al. (2002) |
| | Yukon river Lowlands | 120 | Kasischke et al. (2002) | Brooks Range | 145 | Higuera et al. (2009) |
| | Kuskokwim Mountains | 218 | | | | |
| | Yukon-Tanama Uplands | 330 | | | | |
| | Tanana-Kuskokwim Lowlands | 178 | | | | |
| | Kobuk Ridges and Valleys | 175 | | | | |
| | Davidson Mountains | 403 | | | | |
| | North Ogilive Mountains | 112 | | | | |
| | Ray Mountains | 109 | | | | |
| | Yukon-Old Crow Basin | 81 | | | | |

| | | | | | | |
|---|---|---|---|---|---|---|
| Western North America | Darkwoods, British Columbia | ~69 | Greene and Daniels (2017) | | | |
| | Cascade Mountains, Washington | ~27 | Wright and Agee (2004) | | | |
| | Desolation Peak, Washington Coastal type | 108-137 | | | | |
| | Desolation Peak, Washington Interior type | ~52 | | | | |
| Eastern North America | Quebec – west | ~270* | Bouchard et al. (2008) | Maine | ≥ 800 | Lorimer (1977) |
| | Quebec – east | >500* | | | | |
| | | | | Quebec – "Spruce zone" | 570 | de Lafontaine and Payette (2011) |
| | | | | Quebec – "Fir zone" | >1000 | |
| | Quebec – Abitibi northwest | 418* | Bergeron et al. (2006 post-1940)^ | Quebec – Abitibi northwest | 189 | Bergeron et al. (2006 post-1940)^ |
| | Quebec – Abitibi southwest | 388* | | Quebec – Abitibi southwest | 165 | |
| | Quebec – Abitibi east | 418* | | Quebec – Abitibi east | 141 | |
| | Quebec – Abitibi southeast | 2083* | | Quebec – Abitibi southeast | 257 | |
| | Quebec – Temiscamingue north | 2083* | | Quebec – Temiscamingue north | 220 | |

| | | | | | | |
|---|---|---|---|---|---|---|
| | Quebec – Temiscamingue south | 2777* | | Quebec – Temiscamingue south | 313 | |
| | Quebec – Waswanipi | 418* | | Quebec – Waswanipi | 128 | |
| | Quebec – Central Quebec | 388* | | Quebec – Central Quebec | 150 | |
| | Quebec – North Shore | 645* | | Quebec – North Shore | 281 | |
| | Quebec – Gaspésia | 488* | | Quebec – Gaspésia | 161 | |
| | Quebec – northwestern - lakeshore | 99’ | Bergeron (1991) | Quebec – northwestern - lakeshore | 63’ | Bergeron (1991) |
| | Quebec – northwestern – lake island | 112’ | | Quebec – northwestern – lake island | 74’ | |
| Fennoscandia | Sweden | * | Niklasson and Drakenberg (2001); Niklasson and Granström (2004) | North Sweden | 50-150 | Niklasson and Granström (2004); Niklasson and Granström (2000) |
| | | | | Southern Sweden | 20 | Niklasson and Drakenberg (2001) |
| | Central Sweden | * | Brown and Giesecke (2014) | Central Sweden - Klotjärnen | 180 | Brown and Giesecke (2014) |
| | | | | Central Sweden - Holtjärnen | 240 | |
| Siberian Plateau | Northern | 300 | Kharuk et al. (2016); Kharuk et al. (2011) | | | |
| | Southern | 80 | | | | |
| | Mean (64-71°N) | 110 | | | | |

^ = The reciprocal converted from burn rate (%) (see Van Wagner et al., 2006)

* = Estimates likely effected in some areas by human activity. In such instances Recent Holocene is preferred.

‘ = Fire cycle

†=‘Recent’ here refers to records that (or have distinct sections that) begin after the end of the Holocene Climate Optima and end near present

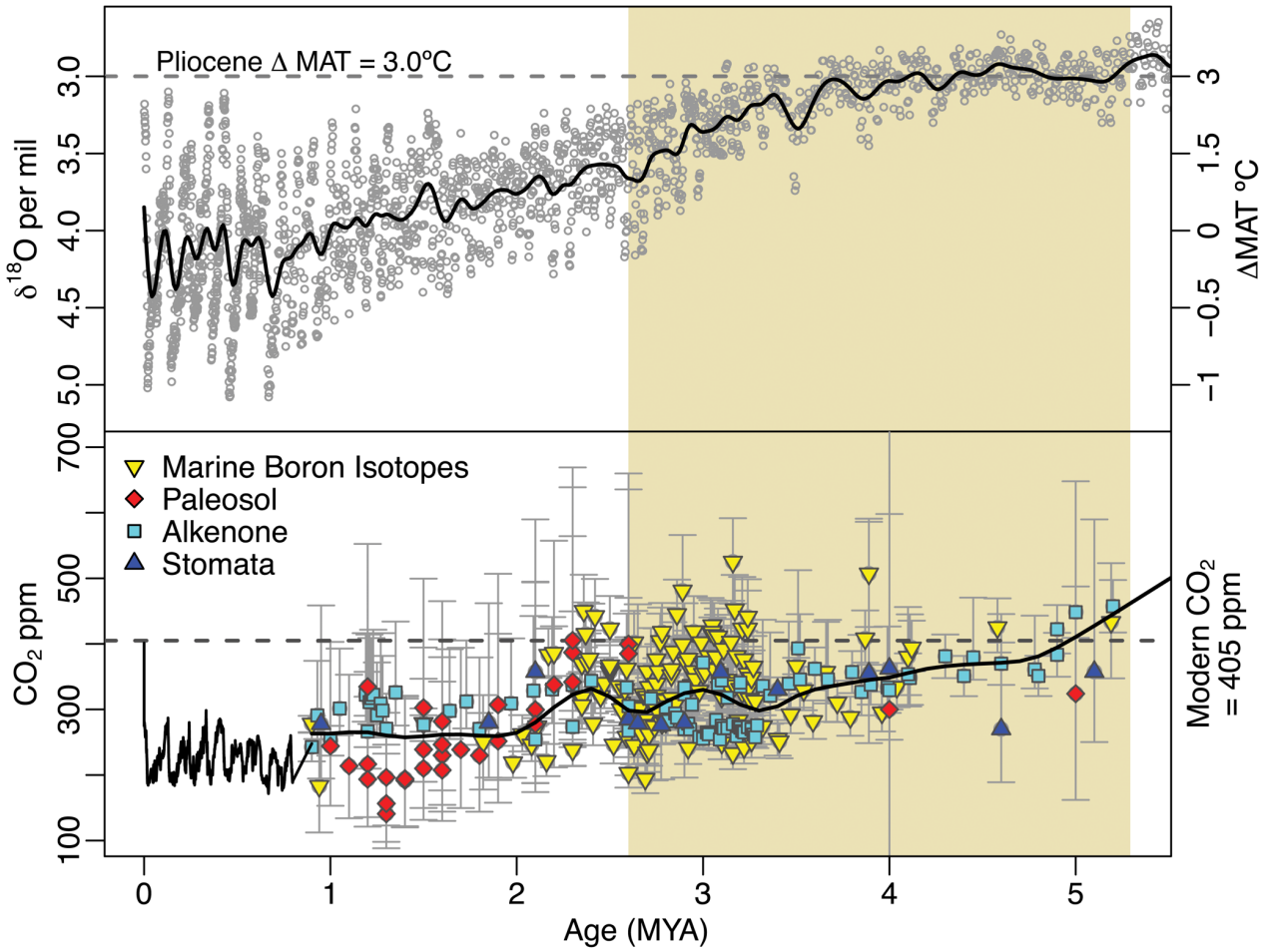


**Figure 1: Global temperatures and atmospheric $CO_2$ concentration spanning the last 5 million years of Earth's history. Mean annual temperatures (MAT) are inferred from compiled $\delta^{18}O$ foraminifera data (Lisiecki and Raymo, 2005) and plotted as anomalies from present (top panel). Modern atmospheric $CO_2$ measurements (NOAA/ESRL), and ice core observations from EPICA (Luthi et al., 2008) are compared with proxy estimates (bottom panel; see Table S1) for the Pliocene Epoch indicated with beige shading. Smoothed curves have been fit to highlight trends in $pCO_2$ and temperature during the Pliocene.**

844

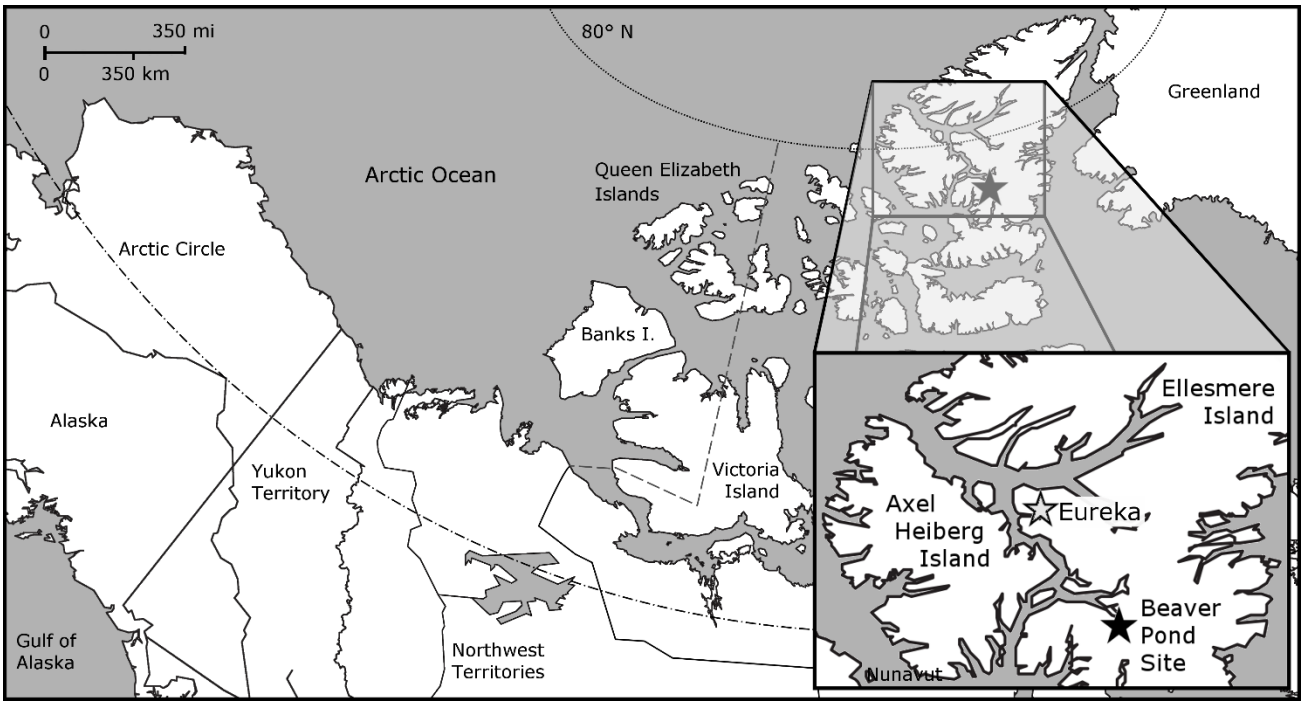


845

846 **Figure 2. Map of the Canadian Arctic Archipelago, highlighting the location of the Beaver Pond Site (Black**
847 **Star; 78° 33′ N; 82° 25′ W) and Eureka Climate Station (Grey Star; 80° 13' N, 86° 11' W – used for modern**
848 **climate comparison) on west-central Ellesmere Island.**

849

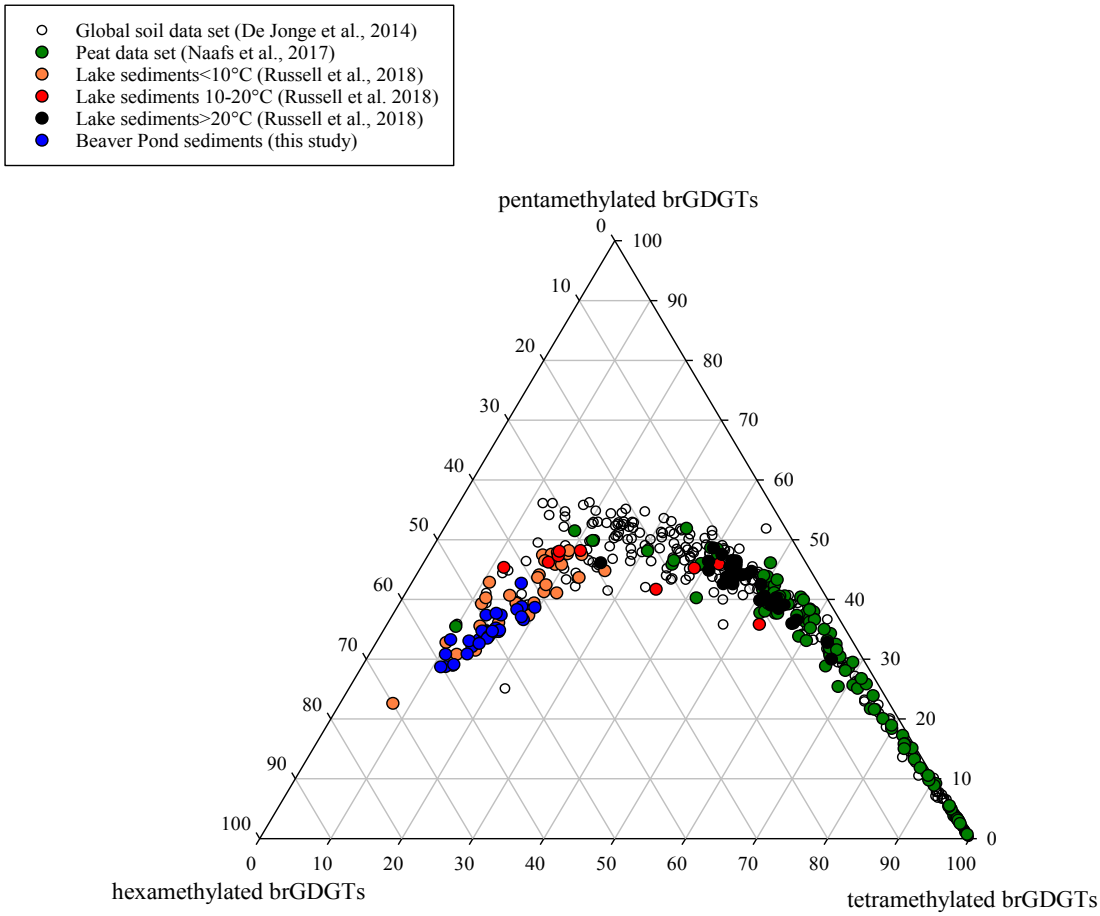


**Figure 3. A ternary plot illustrating the fractional abundances of the tetra- (Ia-c), penta (IIa-c and II′a-c), and hexamethylated (IIIa-c and III′a-c) brGDGTs. The global soil dataset (open circles; De Jonge et al., 2014), the global peat samples (green circles; Naafs et al., 2017), and lake sediments from East Africa (black circles indicate samples from lakes >20°C, red circles indicate samples from lakes between 10–20°C and orange circles designate samples from lakes <10°C; Russell et al., 2018) are included for comparison with the Beaver Pond sediments (blue circles; this study).**

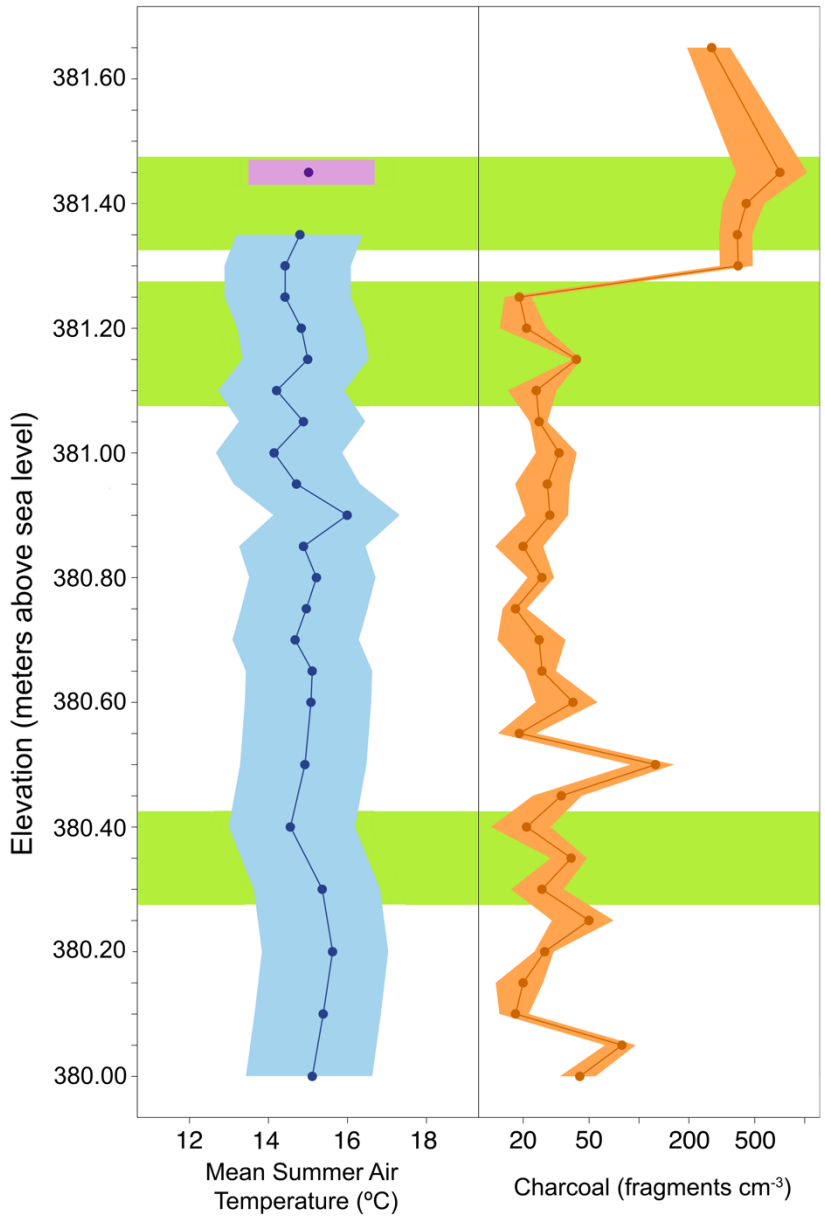


858

859 **Figure 4. Reconstruction of mean summer temperature and fire for the Canadian High Arctic during the**
860 **Pliocene. Mean summer air temperature reconstructed from a brGDGT based proxy (blue; ± 2 σ) and relative**
861 **2010 data point in approximate relative position (purple; ± 2 σ). Charcoal counts reported as the number of**
862 **fragments per volume (fragments $cm^{-3}$) of peat (Orange ± 2 σ). Green boxes indicate relative depths of pollen**
863 **sampling. Elevation of the deposit is reported as meters above sea level. (Data: Table S3)**

**(A)**

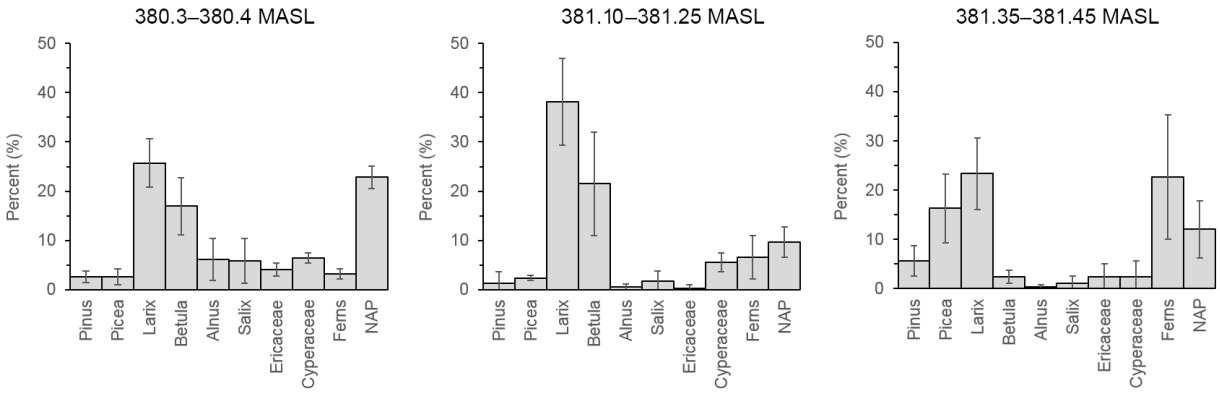


**(B)**

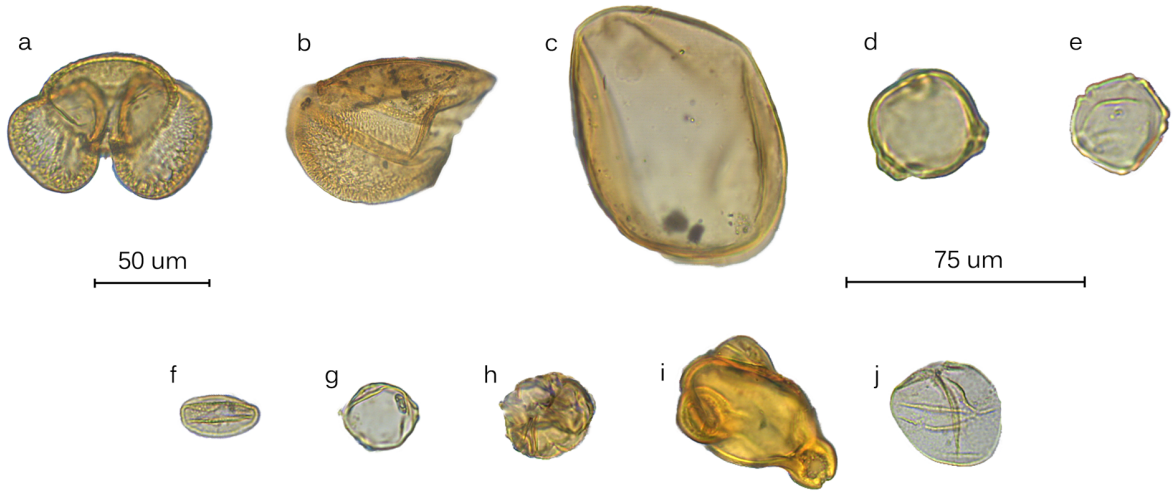


**Figure 5. (A) Bar charts showing the relative pollen abundance in each portion of the section (error bars = 95% confidence intervals; MASL- Meters Above Sea Level). (B). Pollen plate of select grains encountered in the BP section: (a) *Pinus*, (b) half a *Picea* grain, (c) *Larix*, (d) *Betula*, (e) *Alnus*, (f) *Salix*, (g) *Myrica*, (h) ericaceous grain, (i) *Epilobium*, and (j) Cyperaceae. 50um scale = (a–c), 75um scale = (d–j).**

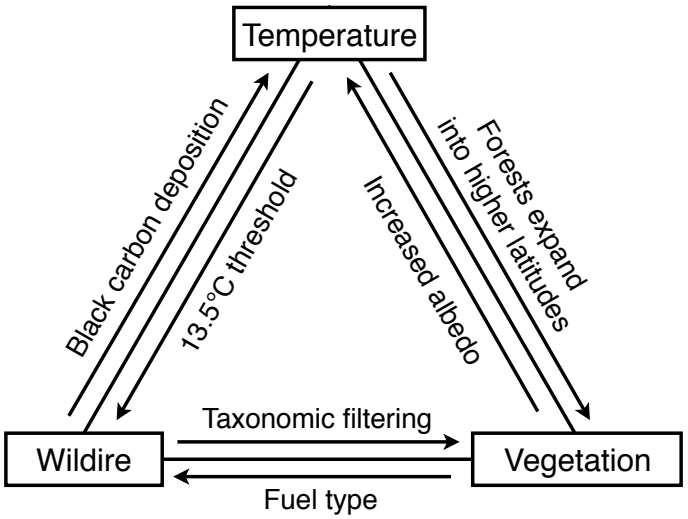


**Figure 6: Examples of the feedbacks between temperature, vegetation and wildfire at the Beaver Pond site**

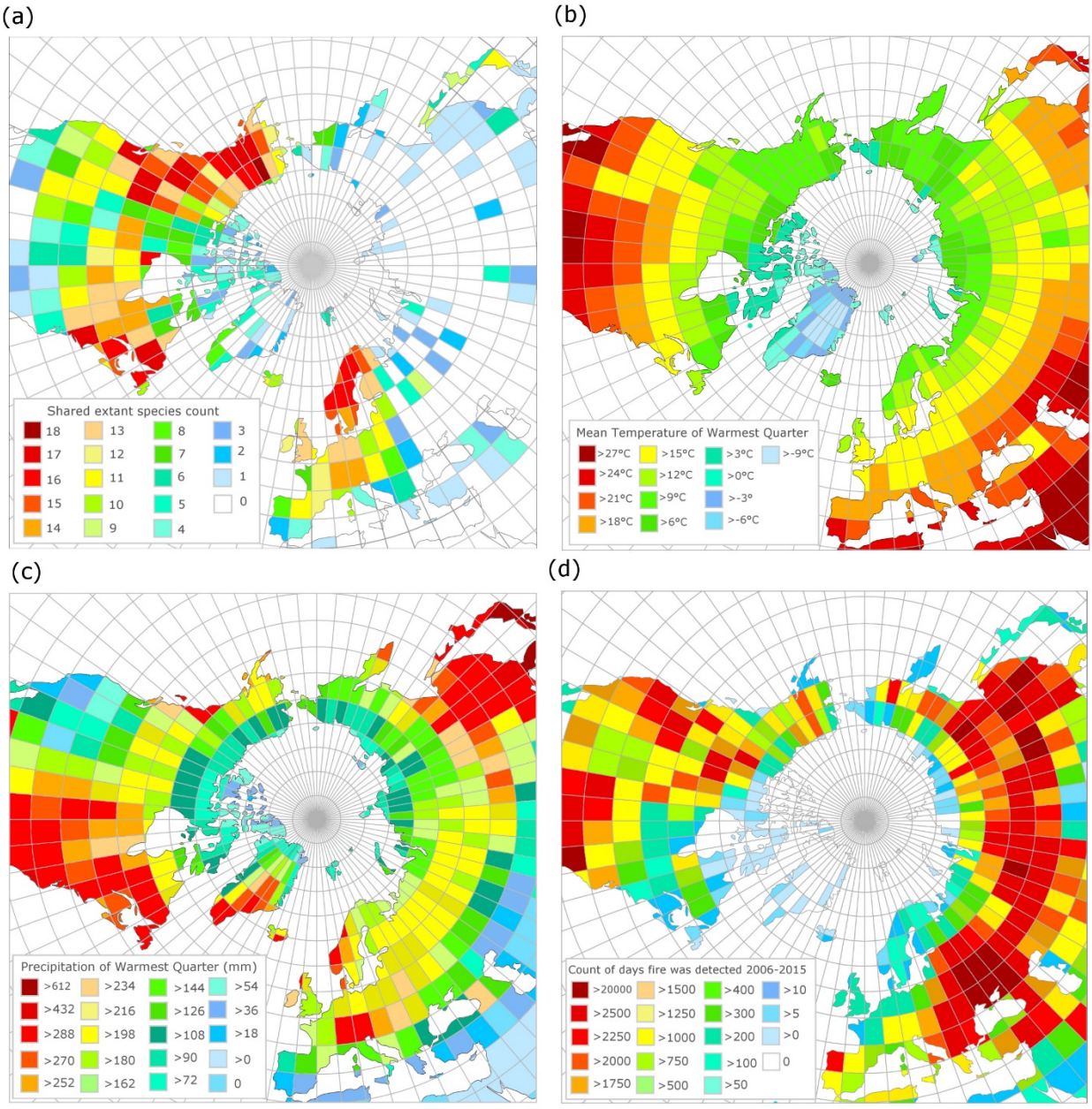


**Figure 7. (a) Modern geographic distribution of observed occurrences of species common to the Beaver Pond species list, (b) Mean temperature of the warmest quarter (summer average) derived from WorldClim, (c) Mean precipitation of the warmest quarter (summer rain) derived from WorldClim, (d) Count of unique fire pixels detected per day, over 10 years from MODIS 6 Fire Product, normalized by area of the latitude by longitude grid.**